Engineering Software Research and Development, Inc.
7750 Clayton Road, Suite 204
St. Louis, MO 63117

Stress/Failure Analysis Software for Multi-Material Interfaces: Final Report

Ricardo L. Actis, Principal Investigator

Project No. FQ8671-9501469 STTR/TS

December 6, 1996

1 Introduction

The objective of the project was to provide means for establishing reliable quantitative failure initiation criteria for multiple chip modules (MCMs), electronic packages, laminated composites and adhesively bonded joints. During Phase I, an easy-to-use, reliable and robust software was developed, with a graphic user interface, based on the innovative methods presented in [1], [2] and [3], for the computation of generalized flux/stress/thermal intensity factors (GFIFs/GSIFs/TSIFs) and the strength of the singularities for any multi-material interface problem involving isotropic or anisotropic materials, subject either to mechanical or thermal loading, in a two-dimensional setting. The existing software product Stress Check provided the framework for this development. Stress Check is based on the p- and hp-version of the finite element method, capable of a-posteriori error estimation in terms of the data of interest.

The specific accomplishments during the Phase I project are summarized below:

- Incorporation of the modified Steklov formulation presented in [1], for computing the strength of the singularities (and the associated eigenfunctions) for the heat-transfer and elasticity problems, into the software product Stress Check.
- Numerical solution of several representative test cases and comparison with known exact solutions to demonstrate the robustness and accuracy of the computation of eigenpairs.
- Implementation of the algorithm for extracting GFIFs and GSIFs. This algorithm, based on the complementary energy principle in conjunction with the p- and hp-versions of the finite element method, is outlined in [2].

- Verification of the accuracy and robustness of the implemented algorithm by computing GFIFs and GSIFs for problems where the exact solution is known.
- Implementation of an algorithm for computing the thermal stress intensity factors (TSIFs), based on the strategy presented in [3].
- Numerical verification of some thermo-elastic problems for which reference solutions are available in the literature.
- Development of a detailed plan for the implementation of this technology in three dimensions. The three- dimensional setting involves vertex singularities, edge singularities and vertex-edge singularities.

The successful completion of these activities made it possible to address the following important questions:

- Which are the characterizing parameters of a thermal, elastic and thermo-elastic solution near a singular point associated with multi-material anisotropic interface problem for any type of singularity? Consequently, what should be changed in the design so as to minimize the likelihood of failure initiation? Given a set of alternatives, which combination of materials is optimal, and which is the best geometric configuration?
- When failure is observed in a device, how should it be modified so as to reduce the likelihood of a future failure?
- How accurate are the parameters that influence failure initiation obtained by the numerical algorithm, i.e., how reliable are the results obtained by numerical simulation? How does the temperature field affect the solution in the vicinity of the singular points?
- How should the analyst interpret the new GFIFs/GSIFs and the "eigenpairs" when correlating with experimental observations?
- How to extend the current two-dimensional capability to three dimensions where the full potential of the technology will be realized?

A detailed description of each activity and the corresponding formulations are given in the next section.

2 Accomplishments

This section describes the activities performed during the Phase I project, in which an easy-to-use, reliable and robust software was developed for the computation of the generalized flux/stress intensity factors and the strength of singularities for multi-material interface problems subjected to thermo-mechanical loads in *two-dimensions*.

The solutions of linear elastostatic and steady-state heat transfer problems in the vicinity of crack tips were an intensive subject of research during the last 30 years. Although an exact solu-

tion can be obtained for cracks in bodies of simple geometries, for most cases involving complex geometries, anisotropic materials, and cracks at bi-material interfaces only a numerical approximation can be obtained. Some typical singular points in an electronic device, for example, where failure initiation commonly occurs, are illustrated in Figure 1.

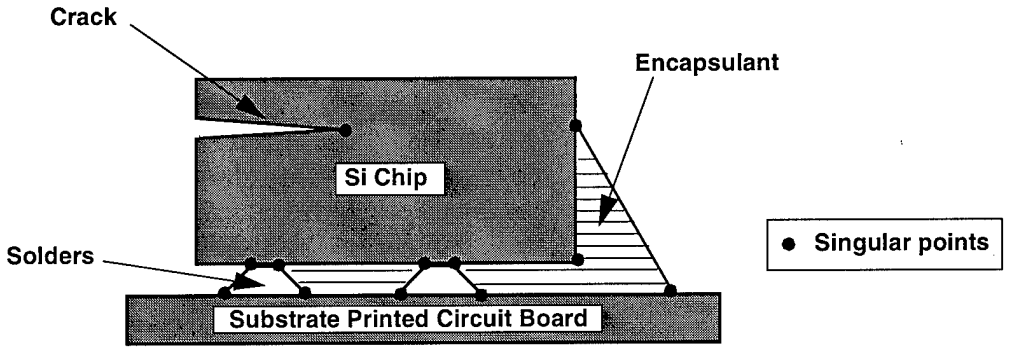

FIGURE 1. Typical sites of failure initiation in an electronic device.

The solution in the vicinity of singular points are of considerable engineering interest (especially for general domains containing multi-material interfaces, and anisotropic materials) because it is directly or indirectly related to failure initiation in composite materials and electronic devices. In the neighborhood of singular points the exact solution of two-dimensional elastostatic problems can be expanded in the form:

$$\{u_{EX}\} = \sum_{i=1}^{\infty} A_i \, r^{\alpha_i} \{\Phi_i(\theta)\} \tag{1}$$

where $\{u_{EX}\}$ is the displacement vector in the x and y directions, r and θ are polar coordinates centered on the singular point; α_i are called eigenvalues and $\phi_i(\theta)$ are called eigenfunctions. These *eigenpairs* (α_i, ϕ_i) depend on the material properties, the geometry and the boundary conditions ($\phi_i(\theta)$ are smooth vector functions). The A_i are coefficients which depend on the loading. Because of their close analogy to stress intensity factors in linear elastic fracture mechanics, A_i are called *generalized stress intensity factors (GSIFs).* In the case of linear steady-state heat transfer problems, the solution in the neighborhood of singular points is analogous to Eq. (1), the differences are that the equation is in a scalar form and the coefficients are called *generalized flux intensity factors (GFIFs).*

For general singular points the exact solution $\{u_{EX}\}$ is generally not know explicitly, i.e., neither the exact eigenpairs nor the exact GFIFs/GSIFs are known, therefore a numerical approximation must be found.

The stresses in the same neighborhood can be computed from the displacements given by Eq. (1) and the material properties as:

$$\{\sigma\} = \sum_{i=1}^{\infty} A_i r^{\alpha_i - 1} \{\psi_i(\theta)\} \tag{2}$$

where $\psi_i(\theta)$ depend on the eigenfunctions in Eq. (1) and the material coefficients. It is clear from Eq. (2) that when $\alpha_i < 1$, the stresses become singular for $r=0$.

The key to successful failure analysis in the presence of singular points is to compute reliably both the eigenpairs and the GSIFs. The eigenvalues characterize the strength of the singularity, the eigenfunctions characterize the straining modes and their amplitudes (the GSIFs/GFIFs) quantify the amount of energy residing in particular straining modes.

A general method for computing the solution in the vicinity of any singular point has been implemented which first determines the eigenpairs, followed by the computation of the GSIFs/ GFIFs for two-dimensional problems. During the Phase I project, the following specific objectives were achieved:

1. Incorporation of the modified Steklov formulation presented in [1], for computing the strength of the singularities (and the associated eigenfunctions) for the heat-transfer and elasticity problems in two-dimensions, into the software product Stress Check.
2. Implementation of the algorithm for extracting the GFIFs and GSIFs. This algorithm, based on the *Complementary Energy Principle* in conjunction with the p- and hp- versions of the finite element method, is outlined in [2].
3. Several representative test cases were solved to demonstrate the robustness and accuracy of the computation of eigenpairs, GFIFs and GSIFs for problems where the exact solution was available.
4. Implementation of an algorithm for computing the thermal stress intensity factors (TSIFs), based on [3] and performance of a thermo-elastic analysis of a typical problem.

2.1 Computation of Eigenpairs

The implementation of the modified Steklov method into Stress Check allows for the computation of the eigenvalues, and the corresponding eigenvectors, for singularities in two-dimensional elastostatic and heat-transfer problems. Once the data are entered into the program, the area

around the selected singular point (but excluding the singular point) is internally divided into finite elements through a meshing process which does not require user intervention. This 'internal mesh' is arranged in a circular ring around the singular point selected by the user in such a way that the element boundaries coincide with the material interfaces. The number of elements of the internal mesh is controlled by the number of material interfaces around the singular point and by the solid angle of the singularity as shown in Figure 2. The largest solid angle for a single element

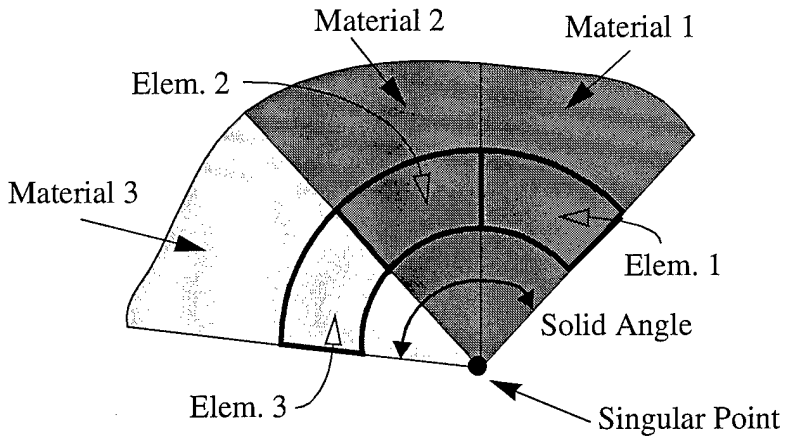

FIGURE 2. Typical 'internal mesh' around singular point in 2D.

is limited to 120°. For each element of the 'internal mesh' we compute the corresponding stiffness and mass matrices. Once the elemental matrices are assembled and the static condensation is performed, the following eigenvalue problem is obtained:

$$[K_S]\{u_R\} = \alpha[M]\{u_R\} \tag{3}$$

where $[K_S]$ is the condensed stiffness matrix; $[M]$ is the mass matrix, and $\{u_R\}$ is the vector of coefficients corresponding to the degrees of freedom associated with the circular boundaries of the 'internal mesh'. The solution of the eigenproblem given by the above equation yields approximation for the eigenvalues α_i and the corresponding eigenvectors. The system of equations is solved for increasing polynomial order to get a converging sequence of solutions (eigenpairs) using routines from the LAPACK library.

The steps and fundamentals for obtaining the system described by Eq. (3) are described in the following.

Consider a domain Ω^*_R shown in Figure 3, in which r, θ are the coordinates of a cylindrical

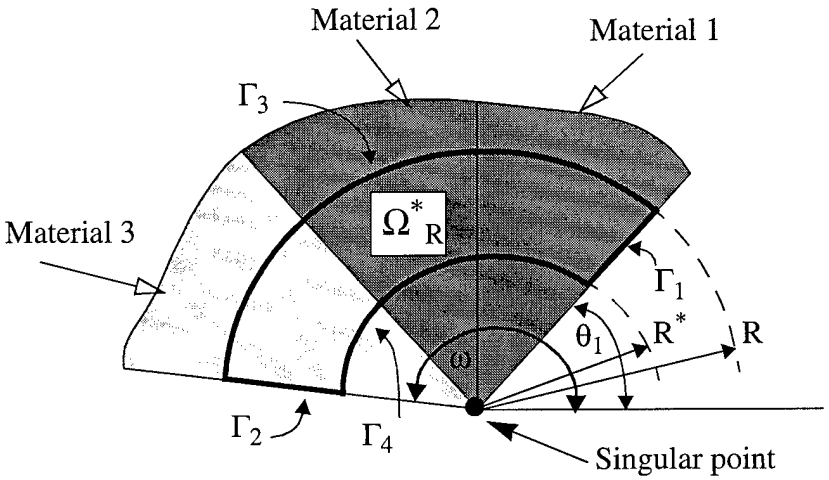

FIGURE 3. Solution domain and notation for the modified Steklov formulation.

coordinate system located in the singular point. By formulating the weak form over Ω^*_R, the singular point is excluded from the domain of interest such that the accuracy of the finite element solution does not deteriorate in its vicinity. On the boundaries Γ_1 and Γ_2 consider either traction-free or zero displacement boundary conditions:

$$\vec{T} = 0 \quad \text{or} \quad \vec{u} = 0 \qquad \text{on } \Gamma_i,\ i = 1, 2. \tag{4}$$

In Ω^*_R, u_x and u_y may be represented as follows:

$$\vec{u} = \begin{Bmatrix} u_x \\ u_y \end{Bmatrix} = r^{\alpha} \begin{Bmatrix} f_1(\theta) \\ f_2(\theta) \end{Bmatrix} \tag{5}$$

Using Eq. (5), on Γ_3:

$$\frac{\partial \vec{u}}{\partial r} = (\alpha/R)\vec{u} \tag{6}$$

and a similar condition on Γ_4.

Multiplying the equilibrium equation by $\vec{v} = \{v_x v_y\}^T \in H^1(\Omega^*_R) \times H^1(\Omega^*_R)$, integrating using Green's theorem, and following the steps presented in [1], the modified Steklov weak form is obtained:

Seek $\alpha \in C, \qquad \vec{0} \neq \vec{u} \in H^1(\Omega^*_R) \times H^1(\Omega^*_R)$

$$B(\vec{u},\vec{v}) - (N_R(\vec{u},\vec{v}) + N_{R^*}(\vec{u},\vec{v})) = \alpha(M_R(\vec{u},\vec{v}) + M_{R^*}(\vec{u},\vec{v})), \qquad \forall\ \vec{v} \in H^1(\Omega_R^*) \times H^1(\Omega_R^*) \tag{7}$$

where C is the complex plane and

$$B(\vec{u},\vec{v}) = \int\int_{\Omega_R^*} ([D]\vec{v})^T [E]([D]\vec{u}) d\Omega, \tag{8}$$

$$M_R(\vec{u},\vec{v}) = \int_\theta [\vec{v}^T [Q][E][R]\vec{u}]_{r=R}\ d\theta, \tag{9}$$

$$N_R(\vec{u},\vec{v}) = \int_\theta [\vec{v}^T [Q][E]([D^{(\theta)}]\vec{u})]_{r=R}\ d\theta, \tag{10}$$

and $[D]$, $[D^{(\theta)}]$, $[Q]$ and $[R]$ are given as follows:

$$[D] = \begin{bmatrix} \frac{\partial}{\partial x} & 0 \\ 0 & \frac{\partial}{\partial y} \\ \frac{\partial}{\partial y} & \frac{\partial}{\partial x} \end{bmatrix}, \qquad [D^{(\theta)}] = \frac{1}{R}\begin{bmatrix} (-\sin\theta)\frac{\partial}{\partial\theta} & 0 \\ 0 & \cos\theta\frac{\partial}{\partial\theta} \\ \cos\theta\frac{\partial}{\partial\theta} & (-\sin\theta)\frac{\partial}{\partial\theta} \end{bmatrix} \tag{11}$$

$$[Q] = \begin{bmatrix} \cos\theta & 0 & \sin\theta \\ 0 & \sin\theta & \cos\theta \end{bmatrix}, \qquad [R] = \begin{bmatrix} \cos\theta & 0 \\ 0 & \sin\theta \\ \sin\theta & \cos\theta \end{bmatrix} \tag{12}$$

and [E] is the material matrix.

Remark 1. The domain Ω^*_R does not include singular edge, hence no special refinement of the finite element mesh is required.

Remark 2. The formulation of the weak form was not based on the assumption that the material is isotropic, and in fact can be applied to multi-material anisotropic interface.

The domain Ω^*_R is divided into finite elements through a meshing process, as described before. The polynomial basis and trial functions, $\{\Phi_j\}$, are defined on a standard element in the ξ, η space such that $-1 < \xi < 1$, $-1 < \eta < 1$. The entries of the unconstrained stiffness matrix corresponding to $B(\vec{u},\vec{v})$ are given by (see Ref. [1]):

$$K_{ij} = \int\int_{\Omega_R^*} ([D]\{\Phi_i\})^T [E][D]\{\Phi_j\} d\Omega \tag{13}$$

For simplicity traction-free boundary conditions are assumed on Γ_1 and Γ_2. Considering first $N(\vec{u},\vec{v}) = N_R(\vec{u},\vec{v}) + N_{R^*}(\vec{u},\vec{v})$, the entries of the matrix $[N_R]$ corresponding to the bilinear form N_R are computed using Gauss quadrature:

$$(N_{ij})_R = \sum_{s=1}^{S} W_s \sum_{l,k=1}^{3} \tilde{P}_{il}(\xi_s) E_{lk} \partial P_{kj}(\xi_s) \tag{14}$$

where W_s and ξ_s are the weights and abscissas of the Gauss quadrature points, respectively, and $\tilde{P}_{il}$ and ∂P_{kj} are matrices given explicitly in [1].

The entries of $[M_R]$ are:

$$(M_{ij})_R = \frac{\omega - \theta_1}{2} \sum_{s=1}^{S} W_s \sum_{l,k=1}^{3} \tilde{P}_{il}(\xi_s) E_{lk} \tilde{P}_{kj}(\xi_s) \tag{15}$$

Expressions similar to Eq. (14) and Eq. (15) exist for the matrices $[N_{R*}]$ and $[M_{R*}]$.

Denoting the set of all coefficients by $\{u_{tot}\}$, and the set of coefficients associated with Γ_3 and Γ_4 by $\{u_R\}$, the following eigenproblem is obtained:

$$([K] - [N_R] - [N_{R^*}])\{u_{tot}\} = \alpha([M_R] + [M_{R^*}])\{u_R\} = \alpha[M]\{u_R\} \tag{16}$$

The vector which represents the total number of nodal values in Ω^*_R can be divided into two vectors such that one contains the coefficients $\{u_R\}$, the other contains the remaining coefficients: $\{u_{tot}\}^T = \{\{u_R\}^T, \{u_{in}\}^T\}$. By eliminating $\{u_{in}\}$, the reduced eigenproblem is obtained:

$$[K_S]\{u_R\} = \alpha[M]\{u_R\} \tag{17}$$

Solution of the eigenproblem given by Eq. (17) yields approximations for eigenpairs with high accuracy, efficiency and robustness.

A new module inside Stress Check allows users to compute the eigenvalues and associated eigenfunctions in a very convenient and easy to use way. The steps necessary to compute the eigenpairs can be summarized as follows:

- First, the model problem is loaded into Stress Check from an existing neutral file or it is created inside the program using the existing pre-processing tools. Stress Check is a p-version finite element analysis program developed by ESRD, Inc. for the solution of elastostatic and heat-transfer problems. It has a Motif-based graphic user interface that allows for the creation of all the geometric features of the problem under consideration. After the geometry was created, the

model can then be meshed, the material properties specified and the boundary conditions imposed. Figure 4a shows a typical two-dimensional model problem displayed in the main window of Stress Check.

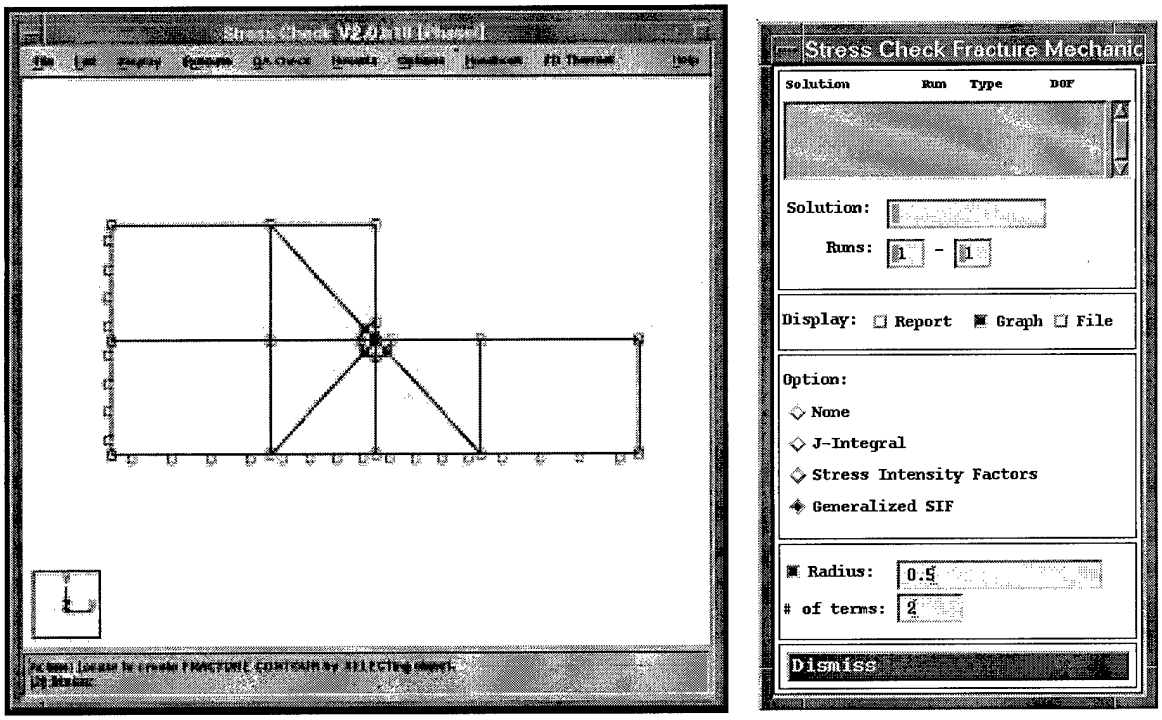

(a) Main Window **(b) Fracture Mechanics dialog box**

FIGURE 4. Stress Check Interface.

- Second, the Fracture Mechanics dialog box is loaded by a menu selection from the main window bar. As shown in Figure 4b, the fracture mechanics options for two-dimensional elasticity are the J-integral, the Stress Intensity Factors and the Generalized Stress Intensity Factor. The first two options are applicable only for cracks in homogeneous materials, and are standard features of Stress Check. The Generalized SIF option has been incorporated as part of this Phase I project
- Finally, to compute the eigenvalues and eigenvectors, the user enters the number of eigenpairs to be computed in the "# of terms" region of the dialog box and then selects the singular point by pointing to it with the cursor and clicking the left button of the mouse. The results are displayed in tabular and/or graphical format depending on the display selection in the dialog box.

The implementation of the modified Steklov method in Stress Check was tested by solving a set of representative benchmark problems for which exact solutions are available in the literature.

Two groups of problems were investigated: Steady state linear heat-transfer problems and linear elastostatic 2D-problems as described in the next sections.

2.1.1 Heat transfer problems

Steady state linear heat-transfer problems (also called scalar problems) in the neighborhood of singular points are considered in this Section. Here u denotes the temperature field in a domain. The governing differential equation is:

$$a_{11}\frac{\partial^2 u}{\partial x^2} + 2a_{12}\frac{\partial^2 u}{\partial x \partial y} + a_{22}\frac{\partial^2 u}{\partial y^2} = 0 \qquad (18)$$

where a_{ij} are the coefficients of heat conduction in each subdomain, with $a_{ij}=a_{ji}$ and the a_{ij} satisfying the elliptic restriction: $a_{11}a_{22} - a_{12}^2 > 0$ in each subdomain. In the case of multimaterial interfaces, it is assumed that the materials are perfectly bonded.

Scalar problem 1: *Isotropic clamped-free crack.* Circular domain of unit radius with a crack along the positive x-axis. One face of the crack (Γ_1) has zero temperature boundary condition and the other face (Γ_2) is flux free. The outside boundary (Γ_R) has an imposed flux (Figure 5)

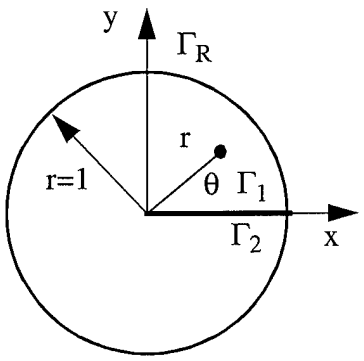

Boundary Conditions:

$u = 0$ on Γ_1; $^{11}\partial u/\partial^{1}\theta = 0$ on Γ_2

$\partial u/\partial r = y$ on Γ_R

FIGURE 5. Scalar problem 1. Notation.

The exact solution for this problem is given by (ref. [4]):

$$u(r,\theta) = -1.35812 r^{1/4}\sin(\theta/4) + 0.970087 r^{3/4}\sin((3\theta)/4) + \ldots \qquad (19)$$

The exact values of the first two eigenvalues for this problem are: $\alpha_1=1/4$ and $\alpha_2=3/4$.

Scalar problem 2: *Anisotropic reentrant corner.* Heat transfer problem in an anisotropic material governed by Eq. (18) with a_{11}=4, a_{12}=0, a_{22}=1. The boundary consists of a 90° reentrant corner generated by two flux-free edges Γ_1 and Γ_2, which meet at the origin of the coordinate system and $u(0,0)$=0 (Figure 6). The circular boundary of the domain (Γ_R) is loaded by flux boundary condi-

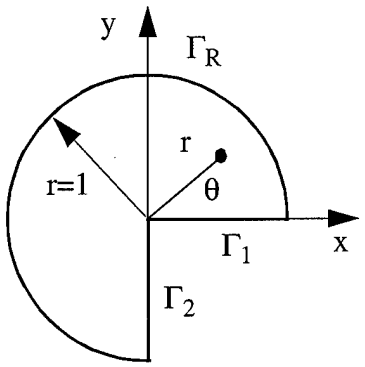

Boundary Conditions:

$u(0,0) = 0$

$\partial u/\partial\theta = 0$ on Γ_1, Γ_2

FIGURE 6. Scalar problem 2. Notation.

tion which corresponds to the first symmetric eigenfunction of the asymptotic expansion of $u(x,y)$ about the reentrant corner (Ref. [9]):

$$q_r = (a_{11}\cos^2\theta + a_{22}\cos^2\theta)\frac{\partial u}{\partial r} + \frac{1}{2}\sin 2\theta(a_{22} - a_{11})\left(\frac{1}{r}\frac{\partial u}{\partial \theta}\right) \tag{20}$$

where the solution $u(r,\theta)$ can be written in the following form:

$$u = \sum_{n=1}^{\infty} A_n r^{\frac{2n}{3}} 2^{-2\frac{n}{3}} (1 + 3\sin^2\theta)^{\frac{n}{3}} \cos\left[\frac{2n}{3}\operatorname{atan}(2\tan\theta)\right] \tag{21}$$

The GFIF A_1 is arbitrarily selected to be A_1=1, while the others are A_i=0, i=2, 3, ... The exact values of the first two eigenvalues are: α_1=2/3 and α_2=4/3.

Scalar problem 3: *Internal interface with two materials.* Two materials perfectly bonded along a common edge satisfying the following equation:

$$p_i \nabla^2 u = 0 \qquad in\ \Omega_i \tag{22}$$

with the following flux conditions along the external boundary (Figure 7):

$$\frac{\partial u}{\partial r} = p_i[\alpha_1 r^{\alpha_1 - 1} h_1(\theta) + \alpha_2 r^{\alpha_2 - 1} h_2(\theta)] \qquad on\ \Gamma_i = \partial\Omega_i \qquad i = 1,2 \tag{23}$$

The material coefficients are: p_1=10, p_2=1; the eigenvalues are: α_1=0.731691779, α_2=1.268308221, and:

$$h_1(\theta) = \begin{cases} \cos[(1-a)\theta] + c_1 \sin[(1-a)\theta] \rightarrow on\ \Gamma_1 \\ c_1 \cos[(1-a)\theta] + c_2 c_3 \sin[(1-a)\theta] \rightarrow on\ \Gamma_2 \end{cases} \quad (24)$$

$$h_2(\theta) = \begin{cases} \cos[(1+a)\theta] - c_3 \sin[(1+a)\theta] \rightarrow on\ \Gamma_1 \\ c_1 \cos[(1+a)\theta] - c_2 c_3 \sin[(1+a)\theta] \rightarrow on\ \Gamma_2 \end{cases} \quad (25)$$

where c_1=6.31818181818182, c_2=-2.68181818181818, c_3=0.64757612580273, and a=0.26830822130025. The exact solution for this problem is (ref. [5]):

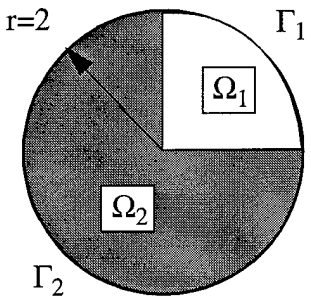

Boundary Conditions:

$\partial u/\partial r = f(r,\theta)$ on Γ_1, Γ_2

FIGURE 7. Scalar problem 3. Notation.

$$u(r,\theta) = A_1 r^{\alpha_1} h_1(\theta) + A_2 r^{\alpha_2} h_2(\theta) \quad (26)$$

where $A_1 = A_2 = 1$.

Results: Figure 8 shows the finite element meshes used for the scalar problems. For problem 1, two layers of geometrically graded elements (with a common factor of 0.15) towards the singular point were used. For problem 2 no geometrically graded meshes were used, while for problem 3 only one layer of elements was placed around the singularity.

The results of the computation of the eigenvalues are summarized in Table 2. For each problem the exact value of the first two eigenvalues, as obtained from the corresponding references, and

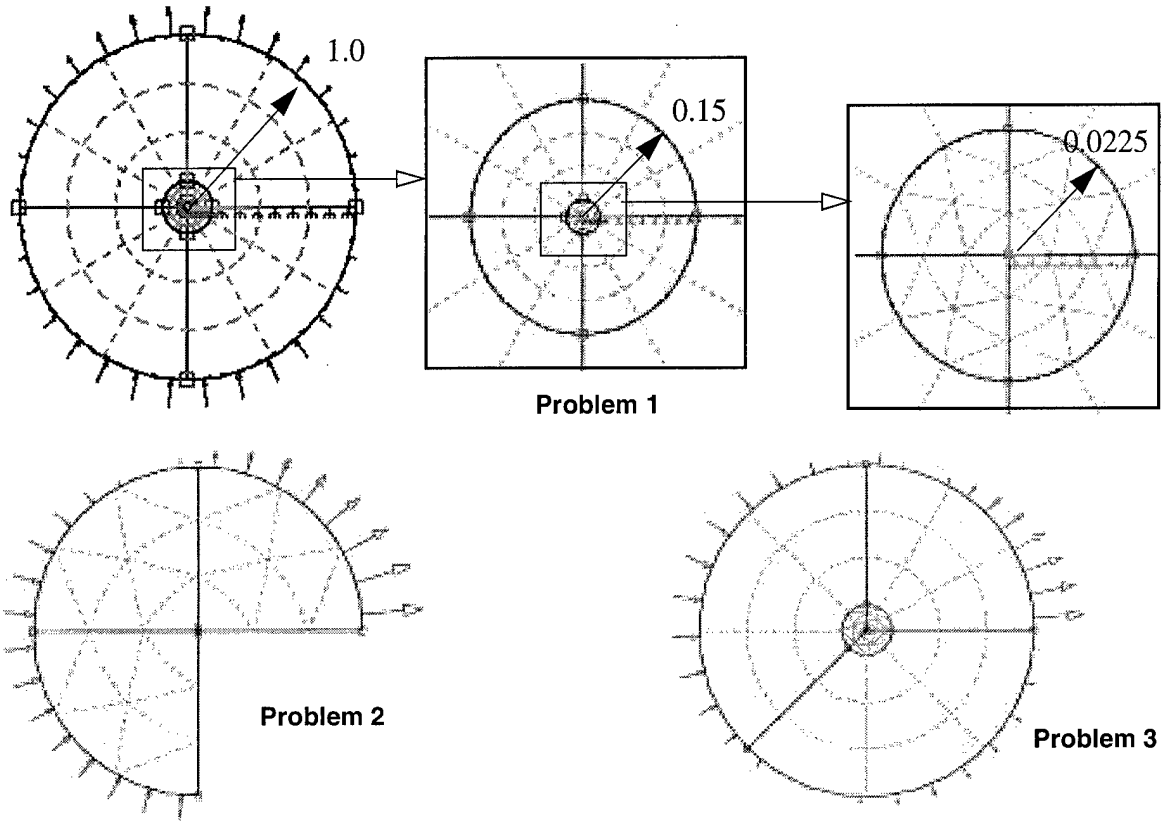

FIGURE 8. Mesh and boundary conditions for scalar problems.

those computed numerically with the modified Steklov method implemented in Stress Check, are included. As the results indicate, the correlation between numerical and exact values is excellent.

TABLE 1. First and second eigenvalues for the scalar model problems

Scalar Problem	First Eigenvalue		Second Eigenvalue	
	Exact	Numerical	Exact	Numerical
1	1/4	0.250000000	3/4	0.750000000
2	2/3	0.666666676	4/3	1.333333308
3	0.731691779	0.731691779	1.268308221	1.268308223

Finally, Figure 9 shows the first eigenfunction as computed in Stress Check for each scalar problem.

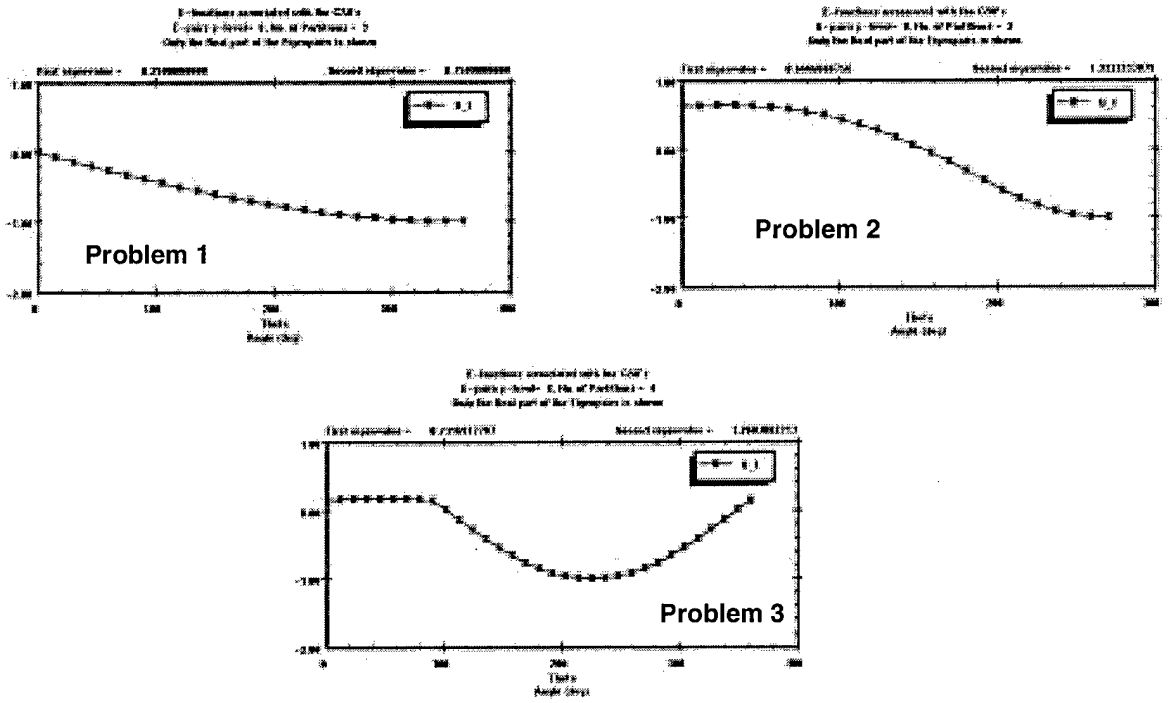

FIGURE 9. First eigenfunction for the scalar problems.

2.1.2 Elastostatic problems

Linear elastostatic model problems in the neighborhood of singular points are considered in this section. Here $\bar{u} = \{u_x, u_y\}^T$ denotes the displacement vector in x, y-directions and σ_x, σ_y and τ_{xy} are the stresses. For multi-material interfaces continuity of displacements and tractions across boundary interfaces is assumed.

Elastostatic problem 1: *Traction-free Isotropic L-shaped domain.* L-Shaped plane elastic body (Figure 10) loaded along the boundaries by the Mode 1 and Mode 2 stress components obtained from the asymptotic expansion of the displacement field about the vertex:

$$\sigma_x = A_1\alpha_1 r^{\alpha_1 - 1} f_1(\theta) + A_2\alpha_2 r^{\alpha_2 - 1} f_2(\theta)$$

$$\sigma_y = A_1\alpha_1 r^{\alpha_1 - 1} g_1(\theta) + A_2\alpha_2 r^{\alpha_2 - 1} g_2(\theta)$$

$$\tau_{xy} = A_1\alpha_1 r^{\alpha_1 - 1} h_1(\theta) + A_2\alpha_2 r^{\alpha_2 - 1} h_2(\theta)$$

where A_1 and A_2 are constants analogous to the mode 1 and mode 2 stress intensity factors in linear elastic fracture mechanics; α_1=0.5444837368 and α_2=0.9085291898 are the first and second eigenvalues; and f_i, g_i, h_i, i=1, 2 are functions of θ given in ref. [6].

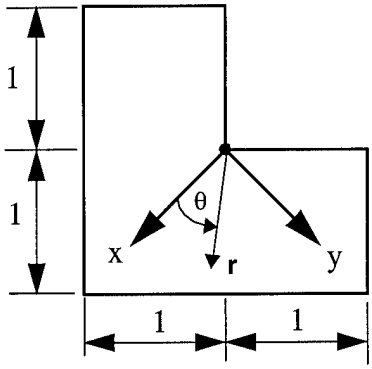

FIGURE 10. Elastostatic problem 1. Notation.

Elastostatic problem 2: *Traction-free crack at an isotropic material interface.* Bi-material interface composed of two homogeneous and isotropic materials with continuity of tractions and displacements across the interface (Figure 11). The body is in a state of plane strain and it is loaded

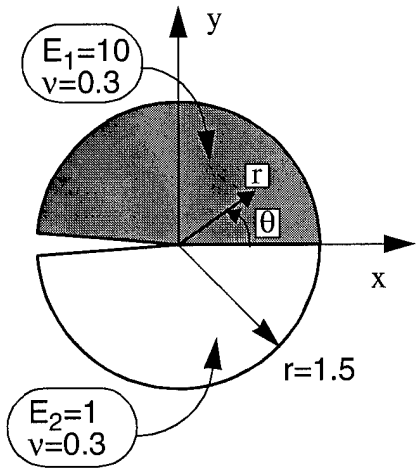

FIGURE 11. Elastostatic problem 2. Notation.

by the stress field corresponding to the exact solution of the asymptotic expansion about the singular point:

$$T_n(r,\theta)\big|_{r=1.5} = \frac{1}{\sqrt{3\pi}}\{K_I[\cos(\varepsilon \ln r)\sigma_{rr}^{\Re} + \sin(\varepsilon \ln r)\sigma_{rr}^{\Im}] + K_{II}[\cos(\varepsilon \ln r)\sigma_{rr}^{\Im} + (-\sin(\varepsilon \ln r))\sigma_{rr}^{\Re}]\}\Big|_{r=1.5}$$

$$T_t(r,\theta)\big|_{r=1.5} = \frac{1}{\sqrt{3\pi}}\{K_I[\cos(\varepsilon \ln r)\sigma_{r\theta}^{\Re} + \sin(\varepsilon \ln r)\sigma_{r\theta}^{\Im}] + K_{II}[\cos(\varepsilon \ln r)\sigma_{r\theta}^{\Im} + (-\sin(\varepsilon \ln r))\sigma_{r\theta}^{\Re}]\}\Big|_{r=1.5}$$

where σ_{rr} and $\sigma_{r\theta}$ are given in ref. [7], K_I and K_{II} are the stress intensity factors and ε is given by:

$$\varepsilon = \frac{1}{2\pi}\ln\left\{\frac{(3-4\nu_1)G_2 + G_1}{(3-4\nu_2)G_1 + G_2}\right\} = 0.07581178$$

where ν is the Poisson's ratio and G is the shear modulus of the material. The first two eigenvalues for this problem are complex: $\underline{\alpha_1 = 0.5 + i\,\varepsilon}$ and $\underline{\alpha_2 = 0.5 - i\,\varepsilon}$.

Elastostatic problem 3: *Inclusion problem.* Composite body consisting of two dissimilar isotropic, homogeneous and elastic wedges, perfectly bonded along the interfaces (Figure 12). The body is loaded by the stress field corresponding to the exact solution of the asymptotic expansion about the singular point as given in ref. [8]. The eigenvalues characterizing the stress singularity

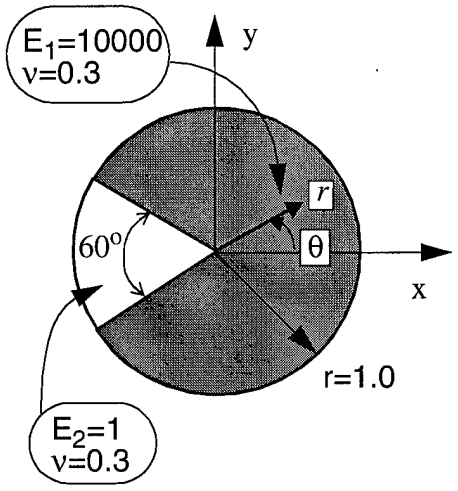

FIGURE 12. Elastostatic problem 3. Notation.

at (0,0) are: $\underline{\alpha_1 = 0.512472160}$ and $\underline{\alpha_2 = 0.730975740}$.

Results: Figure 13 shows the mesh used in solving the elastostatic model problems. For problems 1 and 2, two layers of geometrically graded elements (with a common factor of 0.15) towards the singular point were used. For problem 3 only one layer of elements was placed around the singularity.

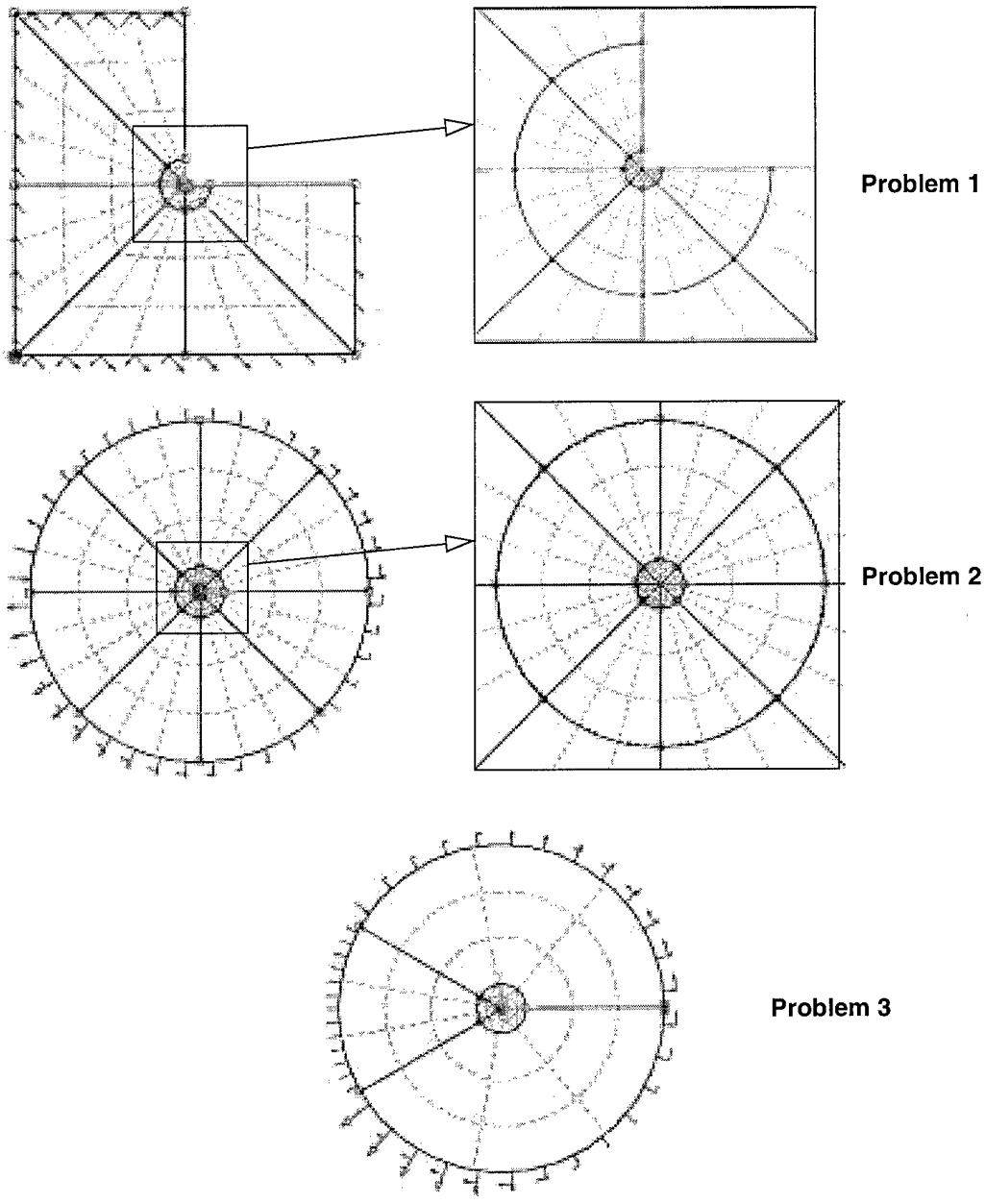

FIGURE 13. Mesh and boundary conditions for elastostatic problems.

The results of the computation of the eigenvalues are summarized in Table 2. For each problem, the exact value of the first two eigenvalues as obtained from the corresponding references, and those computed numerically with the algorithm implemented in Stress Check are included. As the results indicate, the correlation between numerical and exact values is excellent.

TABLE 2. First and second eigenvalues for the elastostatic model problems

Elastostatic Problem	First Eigenvalue		Second Eigenvalue	
	Exact	**Numerical**	**Exact**	**Numerical**
1	0.5444837368	0.5444837375	0.9085291898	0.9085291893
2	0.5+0.07581178*i*	0.5+0.07581178*i*	0.5-0.07581178*i*	0.5-0.07581178*i*
3	0.512472160	0.5124721606	0.730975740	0.7309757404

Finally, Figure 14 shows the first set of eigenfunctions corresponding to problems 1 and 3. They include the eigenfunctions associated with the two displacement components u_x, u_y, and the eigenstresses σ_x, σ_y τ_{xy}.

2.2 Computation of Generalized Flux/Stress Intensity Factors

Once the eigenpairs have been computed, they are used for extracting the GFIFs/GSIFs from the finite element solution. The procedure is described for the case of elasticity. The case of heat transfer is analogous.

After solving the elastostatic problem over the entire domain Ω by means of the finite element method based on the displacement formulation, $\vec{u}_{FE}$ is obtained. A small sub-domain around the singular point is considered next. Defining S_R as the set of interior points of a circle of radius R, centered on the point P, Ω_R is defined by $\Omega \cap S_R$, and Γ_R is the *circular* part of its boundary. See Figure 15.

The complementary variational principle over Ω_R can be stated as:

$$\textbf{Seek } \sigma_0 \in E_c(\Omega_R), \text{ such that}$$

$$B_c(\sigma_0,\sigma_1) = F_c(\sigma_1) \qquad \forall\ \sigma_1 \in E_c(\Omega_R) \tag{27}$$

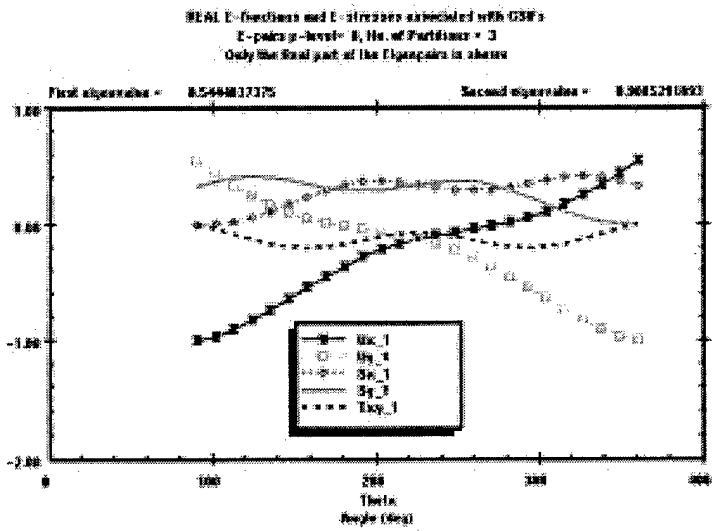

Problem 1

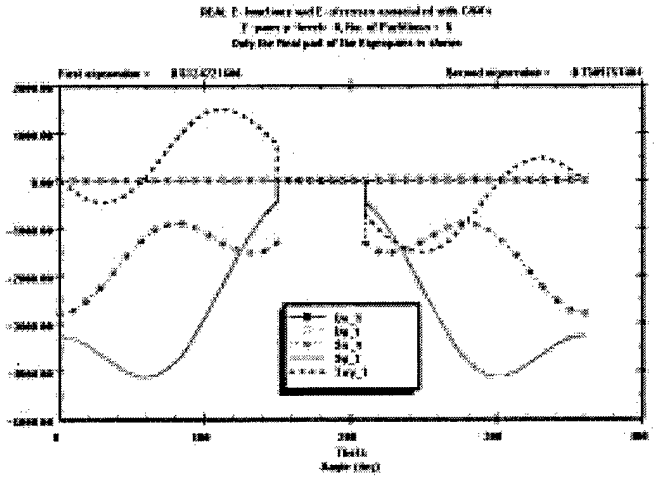

Problem 3

FIGURE 14. Eigenfunctions for elastostatic problems.

$E_c(\Omega_R)$ being the statically admissible space (see a detailed definition in ref. [2]), and $\boldsymbol{B}_c$ and $\boldsymbol{F}_c$ are given by:

$$B_c(\sigma_0,\sigma_1) = \int_{\Omega_R}\int \sigma_0^T[E]^{-1}\sigma_1 d\Omega \tag{28}$$

$$F_c(\sigma_1) = \int_{\partial\Omega_R^{(u)}} \vec{u}^T[Q]\sigma_1 ds \tag{29}$$

where $[E]$ is the material matrix, $\partial\Omega_R{}^{(u)}$ is that part of the boundary where the displacement vector $\vec{u}$ is prescribed, and $[Q]$ is given in Eq. (12).

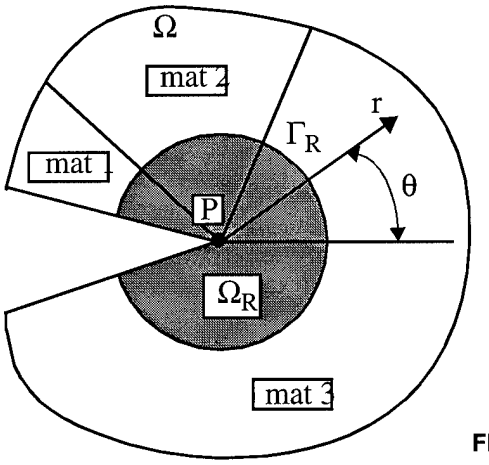

FIGURE 15. Typical singular point P.

For the complementary weak form the trial and test spaces are chosen to be linear combinations of the eigenstresses, which are computed from the eigenpairs, using the stress-strain relationship and Hooke's law. The *ij*-th term of the compliance matrix which corresponds to the bilinear form in Eq. (27) is given by:

$$(B_c)_{ji} = \int_0^R \int_{\theta_1}^{\omega} r^{(\alpha_i^{(R)} + \alpha_j^{(R)} - 1)} \sum_{l,k=1}^{3} (\tilde{D}u)_k^j E_{kl} (\tilde{D}u)_l^i dr d\theta \tag{30}$$

$\alpha_i^{(R)}$ being the real part of the eigenpair, and $(Du)^j$ is a vector corresponding to the *j*-th eigenfunction and is given in ref. [2].

The eigenstress tensor, having been derived from the eigenpairs, automatically satisfies the boundary conditions on all boundaries except Γ_R, so that the linear form in Eq. (29) degenerates into an integral over the circular boundary Γ_R alone.

Replacing the vector u in Eq. (29) with the approximated finite element solution u_{FE} on Γ_3 (see Figure 3), the *j*-th term of the load vector corresponding to the linear form Eq. (29) becomes:

$$(F_c)_j = R \int_{\theta_1}^{\omega} \vec{u}_o^{\,T} [Q][E] \left(\vec{Du}^{(j)} \right) \Big|_{(r=R)} d\theta \tag{31}$$

where $\vec{u}_o = ((u_x^{FE} \cos\theta + u_y^{FE} \sin\theta), (u_x^{FE} \sin\theta + u_y^{FE} \cos\theta))^T$.

Solving Eq. (27), an approximation for the coefficients of the asymptotic expansion (the GSIFs) is obtained. Numerical tests demonstrated that the rate of convergence of the GSIFs is as fast as the convergence of the strain energy, therefore the method is "superconvergent".

The computation of the GFIFs/GSIFs was integrated in Stress Check within the same module described in Section 2.1 for the computation of eigenvalues and associated eigenfunctions for two-dimensional problems in heat transfer and elasticity. The steps to compute the GFIFs/GSIFs are as follows:

- The model problem is loaded into Stress Check from an existing neutral file, or it is created inside the program using the existing pre-processing tools.
- After executing the corresponding analysis (elasticity or heat transfer, depending on the problem), the Fracture Mechanics dialog box is loaded by menu selection from the main window bar.
- The GFIFs/GSIFs is computed by entering the radius of the extraction circle, the number of terms to be computed in the "# of terms" region of the dialog box, and then selecting the singular point by pointing to it with the mouse cursor. The results are displayed in tabular and/or graphical format, depending on the display selection in the dialog box.

A set of benchmark problems for which analytical (exact) solutions are known were investigated. These problems have been selected as representative of the types of singularities present in practical engineering situations associated with linear steady state heat transfer and elastostatic models. The six problems described in Section 2.1.1 and Section 2.1.2 are considered for the computation of GFIFs (scalar problems) and GSIFs (elastostatic problems).

TABLE 3. First and second GFIFs for the scalar problems

Scalar Problem	A_1		A_2	
	Exact	**Numerical**	**Exact**	**Numerical**
1	1.358097	1.328489	0.970087	0.970085
2	1.0	0.998462	0.0	0.000028
3	1.0	1.001243	1.0	1.001222

Table 3 shows the first and second *generalized flux intensity factors* (A_1, A_2) for the heat transfer problems, as computed using the present algorithm and the corresponding exact values. The convergence characteristics of the extraction procedure are illustrated in Figure 16, which shows the values of A_1 and A_2 as a function of the number of degrees of freedom (DOF) for scalar problem 1. As the number of degrees of freedom of the finite element solution is increased, the GFIFs reach a limit value which is practically independent of the discretization.

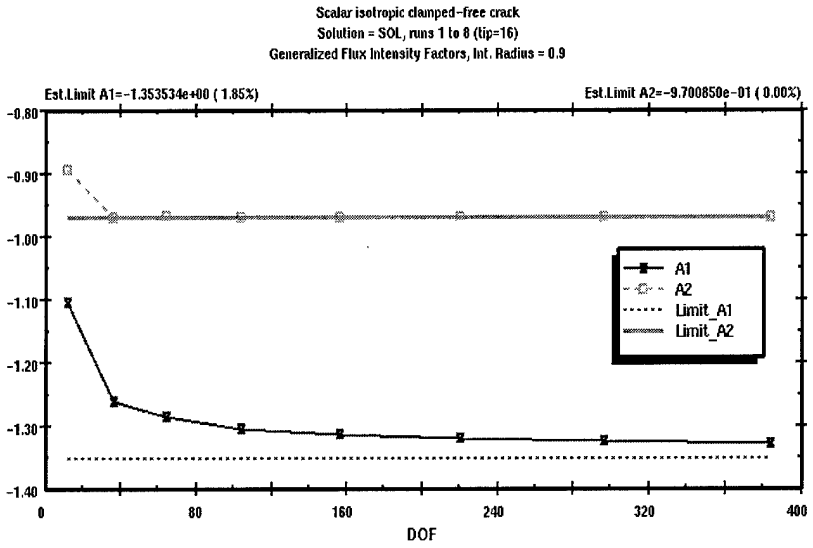

FIGURE 16. Convergence of A1 and A2 for scalar problem 1.

Table 4 shows the first and second *generalized stress intensity factors* (A_1, A_2) for the elastostatic problems. Also included are the corresponding exact values. Figure 17 shows the convergence of the GSIFs for elasticity problem 1 as obtained from Stress Check in tabular and graphical forms.

TABLE 4. First and second GSIFs for the elastostatic model problems

Elasticity Problem	A_1		A_2	
	Exact	**Numerical**	**Exact**	**Numerical**
1	1.0	0.999699	1.0	0.999989
2	1.0	1.000122	1.0	0.999632
3	2.506628	2.508634	2.506628	2.506899

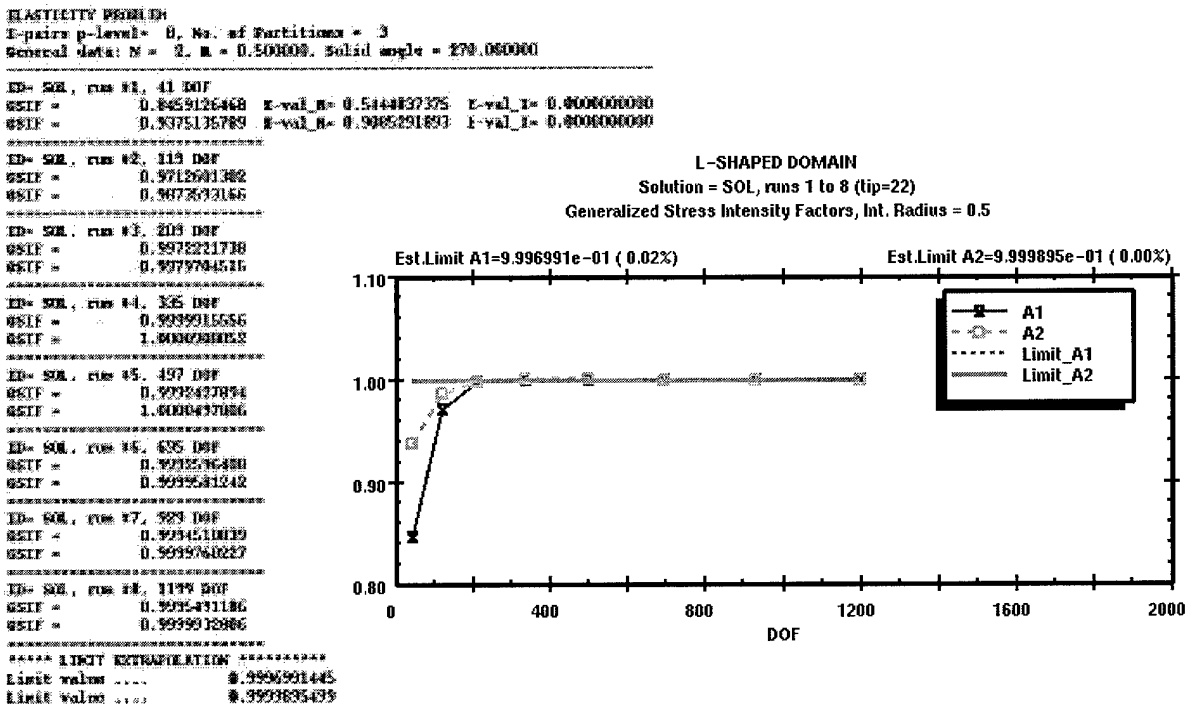

FIGURE 17. Convergence of A1 and A2 for elasticity problem 1.

2.3 Computation of Thermal Stress Intensity Factors

When an elastic body is subjected to thermal loading, the first two coefficients of the asymptotic expansion about the singular points in Eq. (1) are called the thermal stress intensity factors (TSIFs). The computation of the TSIFs can be performed by using the modified Steklov method for the computation of the eigenpairs; the minimum complementary energy principle to obtain the stress intensity factors; and Richardson's extrapolation to determine the TSIFs as the limiting process when $R \rightarrow 0$ (Figure 3). The details of the formulation are available in [3].

To compute the TSIFs, a numerical algorithm was integrated into Stress Check within the same interface as the one used for the computation of the GSIFs. The implementation involves the following steps:

Step 1. *Solve the thermal problem*: Find the temperature distribution over the entire domain given the flux and temperature boundary conditions. Compute the smallest eigenvalue (β_1) associated with the flux singularity by the modified Steklov method as described in Section 2.1.

Step 2. *Solve the thermoelastic problem*: Using the temperature distribution obtained from the solution of the thermal problem as input, obtain the corresponding displacement field of the elasticity problem.

Step 3. *Compute eigenvalues and SIFs:* Extract the first two eigenvalues (α_1, α_2) and the first two stress intensity factors (K_I, K_{II}) from the thermoelastic problem for a given radius (R) of the integration circle. Stress Check will automatically compute the stress intensity factors for three values of the integration circle: $0.9R$, R and $1.1R$.

Step 4. *Compute TSIFs:* Using Richardson's extrapolation, project the three values of each stress intensity factor computed in Step 3 to R=0. The error in the computation of the stress intensity factors is of the order $(R)^q$, where $q=\beta_1-\alpha_1+1$ for the first intensity factor (K_I) and $q=\beta_1-\alpha_2+1$ for the second intensity factor (K_{II}).

The implementation is illustrated with the solution of a representative thermo-elastic problem in two-dimensions.

Central crack in a rectangular plate: Consider a rectangular isotropic plate subjected to two different thermal loadings for which numerical results are available in the literature. The plate of width $2W$, length $2L$ and crack of length $2a=2.0$ with $L/W=1.0$ and $a/W=0.2$ is solved for two thermal loadings representing modes I and II respectively (Figure 18). Since the results are inde-

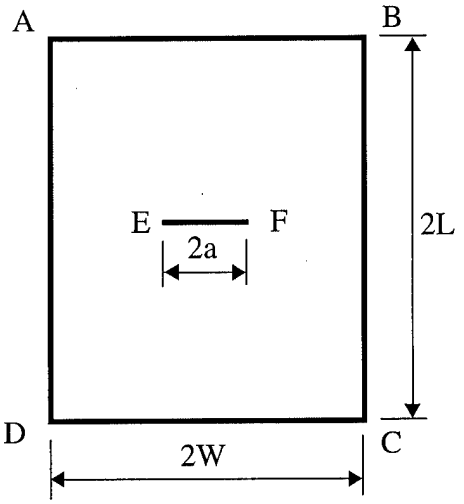

Mode I Loading
AB, BC, CD, DA: **T=100**
EF: **T=0**

Mode II Loading
AB: **T=100**
CD: **T=-100**
BC, DA, EF: $\mathbf{q_n=0}$

FIGURE 18. Plate with central crack. Notation.

pendent of the thermal conductivity for isotropic materials, the heat conduction coefficients are taken as: $a_{11}=a_{22}=1.0$, $a_{12}=0$. The mechanical properties of the material are: Modulus of Elasticity E=1.0; Poisson's ratio ν=0.3; coefficient of thermal expansion α=0.01. Plane-strain conditions are assumed. Because of symmetry, only one half of the plate is analyzed. Figure 19 shows

the finite element mesh used to solve the problem for mode I and mode II loadings. Only one layer of geometrically graded elements towards the crack tip was used in this case.

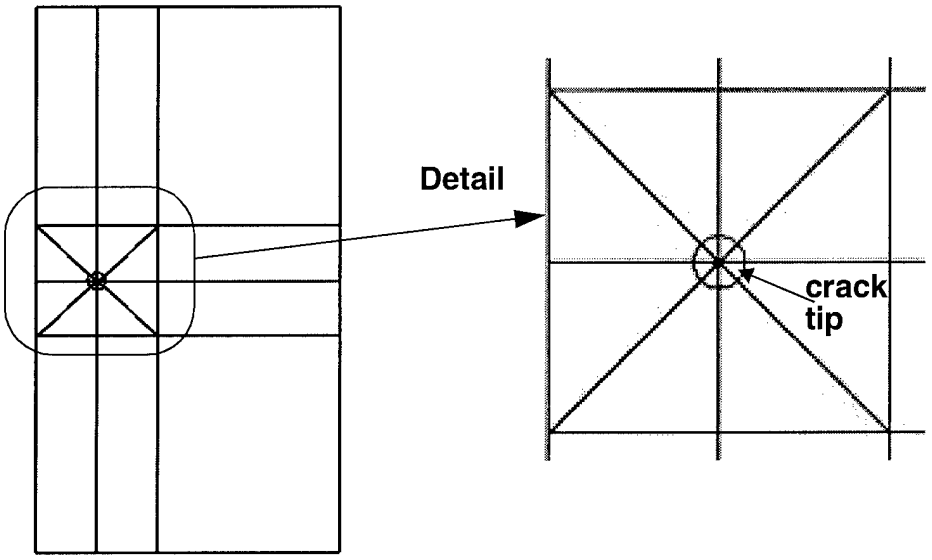

FIGURE 19. Finite element mesh for the plate problem.

The values of the stress intensity factor $K_I^{(0)}$ computed for three radii of the integration circle for Mode I loading are shown in Table 5, together with the values computed using Richardson's

TABLE 5. TSIFs for Mode I loading. Computed and extrapolated values.

R	$K_I^{(0)}$	$K_I^{(1)}$	$K_I^{(2)}$
0.45	1.283830		
		0.809215	
0.50	1.336565		0.79915
		0.811445	
0.55	1.389077		

extrapolation ($K_I^{(1)}$ and $K_I^{(2)}$). For Mode I loading $K_{II}=0$. The smallest eigenvalue associated with the flux singularity was computed to be $\beta_1=0.5$ and the first two eigenvalues associated with the

elasticity singularity are: $\alpha_1=\alpha_2=0.5$. Figure 20 shows the convergence of the mode I TSIF as obtained from Stress Check in tabular and graphical forms, as a function of the number of degrees of freedom (DOF).

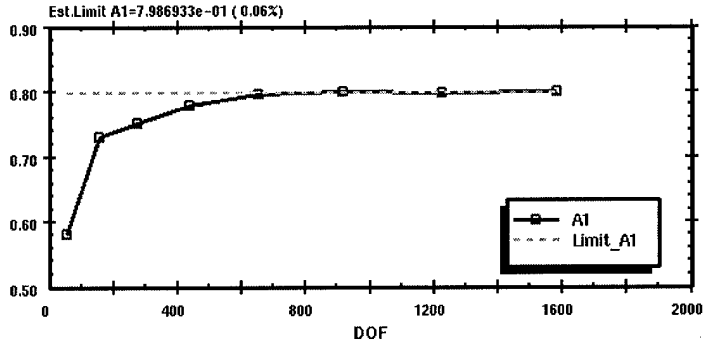


```
==================================
Extrapolated TSIF
DOF      TSIF1          TSIF2
----------------------------------
53       5.815359e-01   1.137471e-14
155      7.314151e-01   9.745229e-16
273      7.524530e-01   -1.761370e-15
439      7.785932e-01   7.229132e-15
653      7.962741e-01   1.814041e-14
915      7.994875e-01   2.199269e-14
1225     7.988002e-01   5.538085e-15
1583     7.991494e-01   5.126567e-15
----------------------------------
```

FIGURE 20. Convergence of Mode I TSIF.

The values of the stress intensity factor $K_{II}^{(0)}$ computed for 3 radii of the integration circle for Mode II loading are shown in Table 6, together with the values computed using Richardson's

TABLE 6. TSIFs for Mode II loading. Computed and extrapolated values.

R	$K_{II}^{(0)}$	$K_{II}^{(1)}$	$K_{II}^{(2)}$
0.45	0.027258		
		0.122953	
0.50	0.016626		0.12170
		0.123231	
0.55	0.005965		

extrapolation ($K_{II}^{(1)}$ and $K_{II}^{(2)}$). For Mode II loading $K_I=0$.

Finally, the extrapolated values of the thermal stress intensity factors K_I (for Mode I loading) and K_{II} (for Mode II loading) are compared with the values published in the literature in Table 7.

TABLE 7. TSIFs for Mode I and II loading. Comparison with references.

	Ref [10]	Ref [11]	Ref [12]	Present Method
K_I	0.8593	0.7759	0.7759	0.7992
K_{II}	0.1317	0.1207	0.1185	0.1217

The numerical example for a crack-tip singularity indicates that the method implemented in Stress Check for the computation of the thermal stress intensity factors is accurate and efficient.

3 Extension to Three-dimensions

The proof of concept completed for two-dimensional problems can be extended to three-dimensional problems that typically occur in the design and manufacture of electronic components. This involves detailed development and implementation of algorithms for the computation of the eigenpairs that characterize the temperature and displacement fields in the vicinity of singularities caused by multi-material interfaces and certain topological details in three dimensions; extraction of the generalized flux and stress intensity factors in three dimensions, and a posteriori estimation of the error in the computed flux and stress intensity factors.

3.1 Objectives

The main goal of Phase I was to develop easy-to-use, reliable and robust software, with a graphical user interface, based on the innovative methods presented in Section 2, for the computation of GFIFs/GSIFs, TSIFs and the strength of singularities for any multi-material interface problem involving isotropic or anisotropic materials, subjected either to mechanical or thermal loading, in a *two-dimensional* setting. The existing software product Stress Check provided the framework for this development. The following specific objectives are considered as an extension of the methods implemented during the Phase I project:

(1) Develop and implement an algorithm for the computation of *eigenpairs* that characterize the *temperature distribution* in the vicinity of singular vertices and edges in multi-material interface problems: Investigate the extension of the Steklov method developed for two-dimensional problems for the computation of eigenpairs in *three-dimensions*. Incorporate into Stress Check the modified Steklov formulation for computing the strength of singularities (and the associated eigenfunctions) for the *heat-transfer problem*.

(2) Develop and implement an algorithm for the computation of the *generalized flux intensity factors* (GFIFs) in the case of steady state heat conduction problems: The algorithm is based on the *Complementary Energy Principle* in conjunction with the p- and hp-versions of the finite element method.

(3) Develop and implement an algorithm for the computation of *eigenpairs* that characterize the *strain distribution* in the vicinity of singular vertices and edges in multi-material interface problems: The modified Steklov formulation for computing the strength of singularities (and the associated eigenfunctions) can be extended for *elasto-static problems* in three-dimensions

(4) Develop and implement an algorithm for the computation of the *generalized stress intensity factors* (GSIFs) when an elastic body is subjected to mechanical loads: The algorithm is based on the *Complementary Energy Principle* in conjunction with the p- and hp-versions of the finite element method.

(5) Develop, implement, test and document an algorithm for computing the *thermo-elastic stress intensity factors* (TSIFs) in three-dimensions.

(6) Develop an algorithm for the coupled thermo-elastic problem accounting for dependence of material properties on temperature in two-dimensions. This will involve:

- Computation of the nonlinear heat transfer solution and investigation of the decomposition of the solution into asymptotic terms.
- Extraction of the generalized flux intensity factors and generalized stress intensity factors for non-constant (temperature dependent) material properties.
- Test implementation and documentation of the algorithms.

Successful completion of these activities will address the following important questions for the most general (three-dimensional) problem:

- What is the thermal, elastic and thermo-elastic solution near a 3D singular point associated with vertex, edge, and vertex-edge multi-material anisotropic interface problem? Consequently, what should be changed in the design so as to minimize the likelihood of failure initiation? Given a set of alternatives, which combination of materials is optimal, and which is the best geometric configuration? Which singularity is worse from th point of view of durability: The vertex, the edge, or the vertex-edge singularity?
- When failure is observed in a device, how should it be modified so as to reduce the likelihood of a future failure? Which mode of failure is to be expected next?
- How accurate are the parameters that influence failure initiation obtained by the numerical algorithm, i.e., how reliable are the results obtained by numerical simulation?
- How does the temperature field affect the solution in the vicinity of singular points in three-dimensions?

- How should the analyst interpret the new GFIFs/GSIFs and the "eigenpairs" when correlating with experimental observations?
- How do the temperature dependent materials influence the singular solution? Consequently, what should be done to prevent or reduce the likelihood of failure initiation and propagation?

Following is a detailed description of the plan for the development and implementation of the activities described above.

3.2 Implementation Plan

Three-dimensional singularities are considerably more difficult to analyze than two-dimensional ones, where only one type of singularity exists. In 3D in a neighborhood of the edges and the vertices the singular behavior is different.

Edge Singularities: If a coordinate system (x,y,z) is located at an edge, with the y-axis along the edge, then there are three edge GSIFs which are y-dependent: $A_I(y)$, $A_{II}(y)$ *and* $A_{III}(y)$. These edge GSIFs are analytic along the edge, however they become singular when this edge intersects with a free plane, at a vertex. In the neighborhood of an edge-vertex type geometry the GSIFs can be represented once again by vertex and vertex-edge stress intensity factors. For example, $A_I(y) = \sum_l S_{I,l} y^{\gamma I, l}$ + *smoother terms.*

Vertex Singularities: In the neighborhood of a vertex, and away from edge-vertex geometry, the displacement field can be represented by only one vertex intensity factor and the corresponding eigenpairs. Investigating the mathematical behavior of the singularities in 3-D is an active field of research in the mathematical community, and the decomposition of the displacement field into singular and regular terms is documented in some recent papers. The application of the modified Steklov method and the complementary energy principle for extracting GSIFs in 3D will be addressed.

3.2.1 Introduction and Notation

The solutions of linear heat-transfer problems in three-dimensions, for example in the vicinity of any singular point, can be decomposed into three different forms, depending whether the singular point is in the neighborhood of an edge, a vertex or an intersection of the edge and the vertex. Mathematical details of the decomposition can be found e.g. in [13]-[16] and the references therein. A representative three-dimensional domain denoted by Ω, which contains typical 3D singular points is shown in Figure 21. Vertex singularities arise in the neighborhood of the vertices A_i, and the edge singularities arise in the neighborhood of the edge singularities Λ_{ij}. Close to the vertex/edge intersection, vertex-edge singularities arise. Of interest is the solution of the mathematical problem:

$$\nabla^2 u = 0 \qquad \text{in } \Omega \tag{32}$$

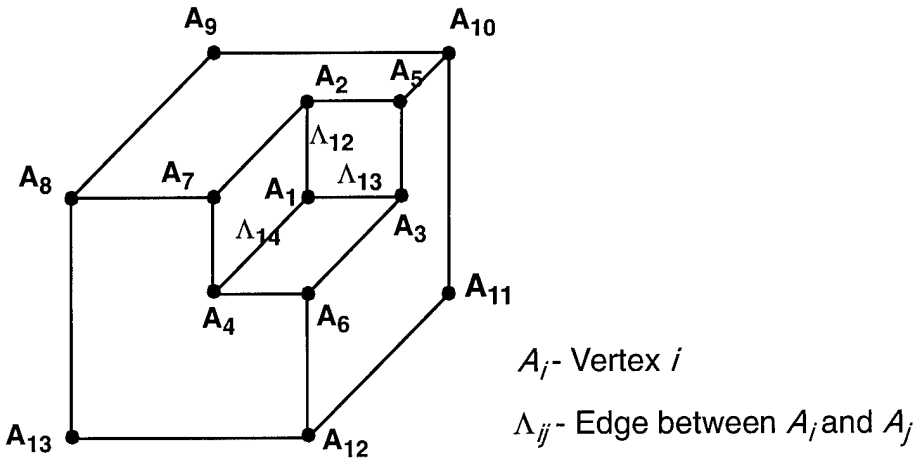

FIGURE 21. Typical 3D singularities.

$$u = 0 \qquad \text{on } \Gamma_D \subset \partial\Omega \tag{33}$$

$$\frac{\partial u}{\partial n} = 0 \qquad \text{on } \Gamma_N \subset \partial\Omega \tag{34}$$

where $u(x_1, x_2, x_3)$ denotes the temperature field (in the following x_1, x_2 and x_3 will be either Cartesian, cylindrical or spherical coordinates), and $\Gamma_D \cup \Gamma_N = \partial\Omega$. It shall be assumed the edges that intersect at vertices are not curved, and that crack faces, if any, lie in a plane.

Edge Singularities: The edges denoted by Λ_{ij}, which connect the vertices A_i and A_j, are considered first. Moving away from the vertex a distance $\delta/2$, and creating a cylindrical subdomain of radius $r = \varepsilon$ with the edge Λ_{ij} as its axis, a subdomain is defined in the vicinity of the edge denoted by $\varepsilon_{\delta,\varepsilon}(\Lambda_{ij})$. Figure 22 shows the edge singularity subdomain $\varepsilon_{\delta,\varepsilon}(\Lambda_{12})$.

The solution in $\varepsilon_{\delta,\varepsilon}$ can be decomposed as follows:

$$\vec{u}(r,\theta,z) = \sum_{k=1}^{K}\sum_{s=0}^{S} a_{ks}(z)\; r^{\alpha_k}(\ln r)^s \vec{f}_{ks}(\theta) \;+\; \vec{v}(r,\theta,z) \tag{35}$$

where $S \geq 0$ is an integer which is zero unless α_k is an integer, $\alpha_{k+1} \geq \alpha_k$ are called edge eigenvalues; $a_{ks}(z)$ are called the edge flux intensity functions (EFIFs), are analytic in z but can become very large as they approach one of the vertices; and $\vec{f}_{ks}(\theta)$, called eigenfunctions, are analytic in θ. The function $\vec{v}(r,\theta,z)$ belongs to $H^2(\varepsilon)$. It is assumed that α_k for $k \leq K$ is not an integer, therefore Eq. (35) becomes:

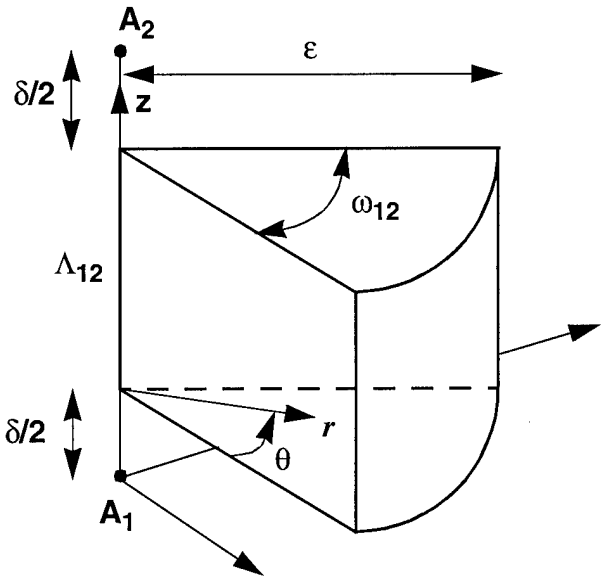

FIGURE 22. The edge neighborhood $\varepsilon_{\delta,\varepsilon}(\Lambda_{12})$.

$$\vec{u}(r,\theta,z) = \sum_{k=1}^{K} a_k(z)\ r^{\alpha_k}\vec{f}_k(\theta) + \vec{v}(r,\theta,z). \tag{36}$$

Vertex Singularities: A ball of radius $\rho = \delta$, centered in the vertex A_1 for example, is constructed and intersected by the domain Ω. Then, a cone having an opening angle $\phi = \sigma$ is constructed along every edge intersecting at A_1, and removed from the previously constructed subdomain, as shown in Figure 23. The resulting vertex subdomain is denoted by $V_\delta(A_1)$, and the solution u can be decomposed in $V_\delta(A_1)$ using a spherical coordinate system by:

$$\vec{u}(\rho,\phi,\theta) = \sum_{l=1}^{L}\sum_{q=0}^{Q} b_{lq}\ \rho^{\gamma_l}(\ln\rho)^q\vec{h}_{lq}(\phi,\theta) + \vec{v}(\rho,\phi,\theta) \tag{37}$$

where $Q \geq 0$ is an integer which is zero unless γ_l is an integer, $\gamma_{l+1} \geq \gamma_l$ are called vertex eigenvalues, and $\vec{h}_{lq}(\phi,\theta)$, called the eigenfunctions, are analytic in ϕ and θ. The b_{lq} are called vertex flux intensity factors (VFIFs). The function $\vec{v}(r,\theta,z)$ belongs to $H^2(V)$. It is assumed that γ_l for $l \leq L$ is not an integer, therefore, Eq. (37) becomes:

$$\vec{u}(\rho,\phi,\theta) = \sum_{l=1}^{L} b_l\ \rho^{\gamma_l}\ \vec{h}_l(\phi,\theta) + \vec{v}(\rho,\phi,\theta) \tag{38}$$

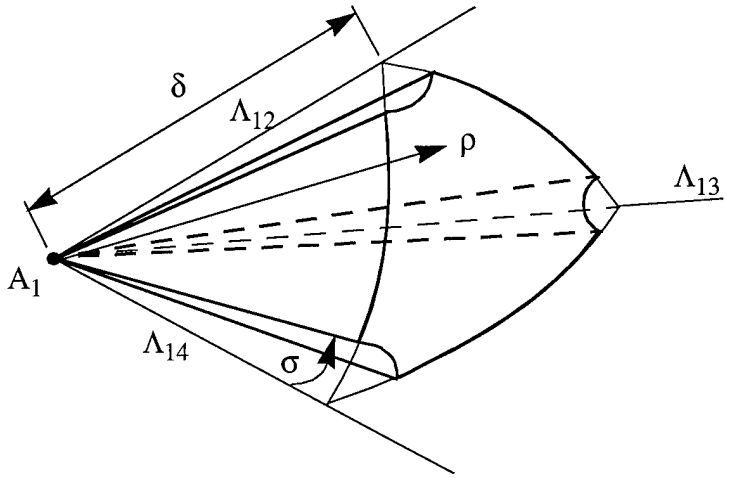

FIGURE 23. The vertex neighborhood $V_\delta(A_1)$.

Vertex-Edge Singularities: The most complicated decomposition of the solution arises in case of vertex-edge intersections. For example, consider the neighborhood where the edge Λ_{12} approaches the vertex A_1. A spherical coordinate system is located in the vertex A_1, and a cone having an opening angle $\phi = \sigma$ with its vertex coinciding with A_1 is constructed with Λ_{12} being its center axis. This cone is terminated by a ball-shaped basis having a radius $\rho = \delta$, as shown in Figure 24. The resulting vertex-edge subdomain is denoted by $V\varepsilon_{\delta,\varepsilon}(A_1, \Lambda_{12})$, and the solution u can be decomposed in $V\varepsilon_{\delta,\varepsilon}(A_1, \Lambda_{12})$:

$$\vec{u}(\rho,\phi,\theta) = \sum_{k=1}^{K}\sum_{s=0}^{S}\left(\sum_{l=1}^{L} a_{ksl}\ \rho^{\gamma_l} + m_{ks}(\rho)\right)(\sin\phi)^{\alpha_k}[\ln(\sin\Phi)]^s \vec{g}_{ks}(\theta) + \sum_{l=1}^{L}\sum_{q=0}^{Q} c_{lq}\rho^{\gamma_l}(\ln\rho)^q \vec{h}_{lq}(\phi,\theta) + \vec{v}(\rho,\phi,\theta) \tag{39}$$

where $m_{ks}(\rho)$ is analytic in ρ; $\vec{g}_{ks}(\theta)$ is analytic in θ, and $\vec{h}_{lq}(\phi,\theta)$ is analytic in ϕ and θ. The function $\vec{v}(r, \theta,z)$ belongs to $H^2(V\varepsilon)$. Again it is assumed that γ_l for $l \le L$ is not an integer, and α_k for $k \le K$ is not an integer, therefore, Eq. (39) becomes:

$$\vec{u}(\rho,\phi,\theta) = \sum_{k=1}^{K}\left(\sum_{l=1}^{L} a_{kl}\ \rho^{\gamma_l} + m_k(\rho)\right)(\sin\phi)^{\alpha_k}\vec{g}_k(\theta) + \sum_{l=1}^{L} c_l\ \rho^{\gamma_l}\ \vec{h}_l(\phi,\theta) + \vec{v}(\rho,\phi,\theta) \tag{40}$$

The eigenvalues and the eigenfunctions are associated pairs (eigenpairs) which depend on the material properties, the geometry, and the boundary conditions *in the vicinity of the singular point/ edge only.* Similarly, the solution for problems in linear elasticity, in the neighborhood of singular points/edges is analogous to Eq. (35)-Eq. (40), the differences are that the equations are in vector form and the eigenpairs may be complex. For general singular points the exact solution u_{EX} is

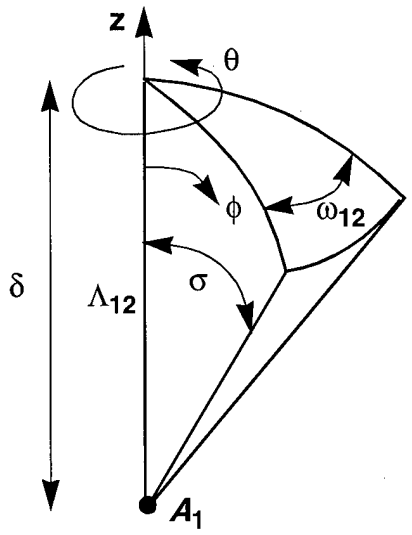

FIGURE 24. The vertex-edge neighborhood $V\varepsilon_{\delta,\varepsilon}(A_1, \Lambda_{12})$.

generally not known explicitly, i.e., neither the exact eigenpairs nor the exact EFIFs, VFIFs are known, therefore numerical approximations must be found.

3.2.2 Determination of the Eigenpairs

First, the modified Steklov method for determining the eigenpairs in the neighborhood of the singular point is described. Herein the formulation for the elastic problem is provided for the case of the edge singularity described in Section 3.2.1. The formulation for the heat-transfer problem is similar but much less complex, therefore not presented herein. Consider the domain Ω^*_R shown in Figure 25, which represents a cross-section of an edge singularity, and where r, θ are the coordinates of a cylindrical coordinate system located in the singular edge.

By formulating the weak form over Ω^*_R, the singular edge is excluded from the domain of interest such that the accuracy of the finite element solution does not deteriorate in its vicinity. On the boundaries Γ_1 and Γ_2 traction-free or zero displacement boundary conditions are assumed:

$$\vec{T} = 0 \quad \text{or} \quad \vec{u} = 0 \qquad \text{on } \Gamma_i,\ i=1,2,3 \tag{41}$$

In Ω^*_R, u_x, u_y and u_z may be represented as follows:

$$\vec{u} = \begin{Bmatrix} u_x \\ u_y \\ u_z \end{Bmatrix} = r^{\alpha} \begin{Bmatrix} f_1(\theta) \\ f_2(\theta) \\ f_3(\theta) \end{Bmatrix} \tag{42}$$

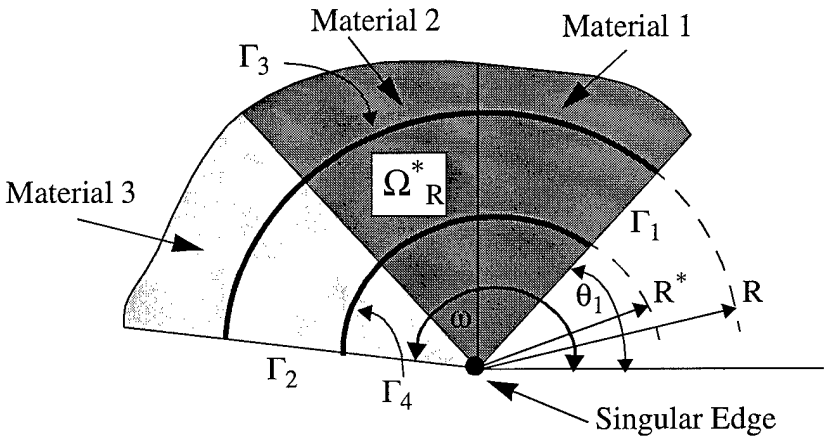

FIGURE 25. Cross section of an edge singularity for the modified Steklov formulation.

Using Eq. (42) on Γ_3:

$$\frac{\partial}{\partial r}\vec{u} = (\alpha/R)\vec{u} \tag{43}$$

and a similar condition on Γ_4.

Multiplying the equilibrium equation by $\vec{v} = \{v_x, v_y, v_z\}^T \in H^1(\Omega^*_R) \times H^1(\Omega^*_R)$, integrating using Green's theorem, and following the steps presented in Ref. [1], the modified Steklov weak form is:

$$\textbf{Seek} \qquad \alpha \in C, \qquad \vec{0} \neq \vec{u} \in H^1(\Omega^*_R) \times H^1(\Omega^*_R)$$

$$B(\vec{u},\vec{v}) - (N_R(\vec{u},\vec{v}) + N_{R^*}(\vec{u},\vec{v})) = \alpha(M_R(\vec{u},\vec{v}) + M_{R^*}(\vec{u},\vec{v})), \qquad \forall\ \vec{v} \in H^1(\Omega^*_R) \times H^1(\Omega^*_R) \tag{44}$$

where C is the complex plane and

$$B(\vec{u},\vec{v}) = \int_z \iiint_{\Omega^*_R} ([D]\vec{v})^T [E]([D]\vec{u}) d\Omega dz, \tag{45}$$

$$M_R(\vec{u},\vec{v}) = \int_z \iint_\theta [\vec{v}^T [Q][E][R]\vec{u}]_{r=R}\ d\theta dz, \tag{46}$$

$$N_R(\vec{u},\vec{v}) = \int_z \iint_\theta [\vec{v}^T [Q][E]([D^{(\theta)}]\vec{u})]_{r=R}\ d\theta dz, \tag{47}$$

and $[D]$, $[D^{(\theta)}]$, $[Q]$ and $[R]$ are given as follows:

$$[D] = \begin{bmatrix} \frac{\partial}{\partial x} & 0 & 0 \\ 0 & \frac{\partial}{\partial y} & 0 \\ 0 & 0 & \frac{\partial}{\partial z} \\ \frac{\partial}{\partial y} & \frac{\partial}{\partial x} & 0 \\ 0 & \frac{\partial}{\partial z} & \frac{\partial}{\partial y} \\ \frac{\partial}{\partial z} & 0 & \frac{\partial}{\partial x} \end{bmatrix}, \qquad [D^{(\theta)}] = \frac{1}{R}\begin{bmatrix} (-\sin\theta)\frac{\partial}{\partial\theta} & 0 & 0 \\ 0 & \cos\theta\frac{\partial}{\partial\theta} & 0 \\ 0 & 0 & 0 \\ \cos\theta\frac{\partial}{\partial\theta} & (-\sin\theta)\frac{\partial}{\partial\theta} & 0 \\ 0 & 0 & \cos\theta\frac{\partial}{\partial\theta} \\ 0 & 0 & (-\sin\theta)\frac{\partial}{\partial\theta} \end{bmatrix} \tag{48}$$

$$[Q] = \begin{bmatrix} \cos\theta & 0 & 0 & \sin\theta & 0 & 1 \\ 0 & \sin\theta & 0 & \cos\theta & 1 & 0 \\ 0 & 0 & 1 & 0 & \sin\theta & \cos\theta \end{bmatrix}, \qquad [R] = \begin{bmatrix} \cos\theta & 0 & 0 \\ 0 & \sin\theta & 0 \\ 0 & 0 & 0 \\ \sin\theta & \cos\theta & 0 \\ 0 & 0 & \sin\theta \\ 0 & 0 & \cos\theta \end{bmatrix} \tag{49}$$

and [E] is the material stiffness matrix.

Remark 1. The domain Ω^*_R does not include a singular edge, hence no special refinement of the finite element mesh is required.

Remark 2. The formulation of the weak form was not based on the assumption that the material is isotropic, and in fact can be applied to multi-material anisotropic interface.

The domain Ω^*_R is divided into finite elements through a meshing process. The polynomial basis and trial functions, $\{\Phi_j\}$, are defined on a standard element in the ξ, η, ζ space such that $-1 < \xi < 1$, $-1 < \eta < 1$, $-1 < \zeta < 1$. The entries of the unconstrained stiffness matrix corresponding to $B(\vec{u},\vec{v})$ are given by (see Ref. [1]):

$$K_{ij} = \int_z \iint_{\Omega^*_R} ([D]\{\Phi_i\})^T [E][D]\{\Phi_j\} d\Omega dz \tag{50}$$

For simplicity, on Γ_1 and Γ_2 traction-free boundary conditions are assumed. Consider first $N(\vec{u},\vec{v}) = N_R(\vec{u},\vec{v}) + N_{R^*}(\vec{u},\vec{v})$. The entries of the matrix $[N_R]$ corresponding to the bilinear form N_R are computed using Gauss quadrature:

$$(N_{ij})_R = \sum_{s=1}^{S}\sum_{t=1}^{T} W_s W_t \sum_{l,k=1}^{6} \tilde{P}_{il}(\xi_s,\eta_t) E_{lk} \partial P_{kj}(\xi_s,\eta_t) \tag{51}$$

where W_s, W_t, are the weights and ξ, η are the abscissas of the Gauss quadrature points, respectively, and $\tilde{P}_{il}$ and ∂P_{kj} are matrices given explicitly in Ref. [1].

The entries of $[M_R]$ are:

$$(M_{ij})_R = \frac{\omega - \theta_1}{2} \sum_{s=1}^{S}\sum_{t=1}^{T} W_s W_t \sum_{l,k=1}^{6} \tilde{P}_{il}(\xi_s,\eta_t) E_{lk} \tilde{P}_{kj}(\xi_s,\eta_t) \tag{52}$$

Expressions similar to Eq. (51) and Eq. (52) exist for the matrices $[N_{R*}]$ and $[M_{R*}]$.

Denoting the set of all coefficients by $\{u_{tot}\}$, and the set of coefficients associated with Γ_3 and Γ_4 by $\{u_R\}$, the following eigenproblem is obtained:

$$([K] - [N_R] - [N_{R^*}])\{u_{tot}\} = \alpha([M_R] + [M_{R^*}])\{u_R\} = \alpha[M]\{u_R\} \tag{53}$$

The vector which represents the total number of nodal values in Ω^*_R can be divided into two vectors such that one contains the coefficients $\{u_R\}$, the other contains the remaining coefficients: $\{u_{tot}\}^T = \{\{u_R\}^T, \{u_{in}\}^T\}$. By eliminating $\{u_{in}\}$, the reduced eigenproblem is obtained:

$$[K_S]\{u_R\} = \alpha[M]\{u_R\} \tag{54}$$

Solution of the eigenproblem given by Eq. (54) yields approximations for eigenpairs with high accuracy, efficiency and robustness.

3.2.3 Extraction of the GSIFs.

Once the eigenpairs have been computed, they are used for extracting the GSIFs from the finite element solution. The procedure is as follows: First the elastostatic problem is solved over the entire domain Ω by means of the finite element method based on the displacement formulation, thus obtaining $\vec{u}_{FE}$. Second, a small sub-domain around the singular edge is considered. Define S_R as the set of interior points of a circle of radius R, centered on the point P. Ω_R is defined by $\Omega \cap R_R \times I_z$, where I_z is a segment along the edge: $I_z = \{z \mid z_1 \le z \le z_2\}$ and Γ_R is the *circular* part of its boundary. See Figure 26.

The complementary variational principle over Ω_R can be stated as:

Seek $\sigma_0 \in E_c(\Omega_R)$, such that

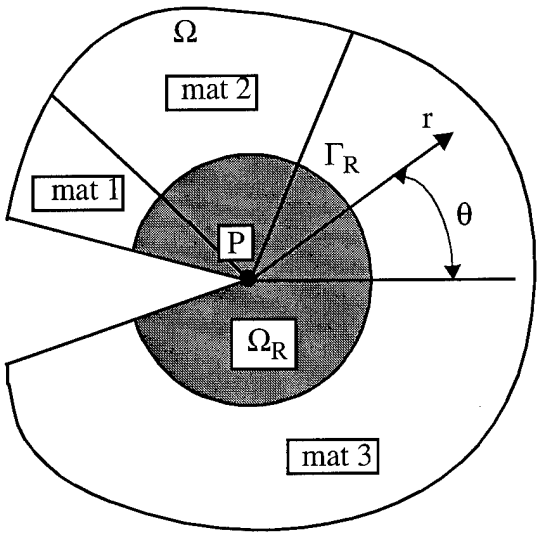

FIGURE 26. Typical cross-section of an edge singularity.

$$B_c(\sigma_0,\sigma_1) = F_c(\sigma_1) \qquad \forall\ \sigma_1 \in E_c(\Omega_R) \tag{55}$$

$E_c(\Omega_R)$ being the statically admissible space (see a detailed definition in Ref. [2]), and $\boldsymbol{B}_c$ and $\boldsymbol{F}_c$ are given by:

$$B_c(\sigma_0,\sigma_1) = \int_{I_z}\int_{\Omega_R} \sigma_0^T [E]^{-1} \sigma_1 \, d\Omega dz \tag{56}$$

$$F_c(\sigma_1) = \int_{I_z}\int_{\partial\Omega_R^{(u)}} \vec{u}^T [Q] \sigma_1 \, ds dz \tag{57}$$

where $[E]$ is the material matrix, $\partial\Omega_R{}^{(u)}$ is that part of the boundary where the displacement vector $\vec{u}$ is prescribed, and $[Q]$ is given in Eq. (49).

For the complementary weak form the trial and test spaces are chosen to be linear combinations of the eigenstresses, which are computed from the eigenpairs, using the stress-strain relationship and Hooke's law. In the three-dimensional case it has to be recognized that the stress intensity factor is a function of z. Therefore the stress intensity is discretized using polynomial basis functions which are energy orthogonal on the interval I_z.

The ij-th term of the compliance matrix which corresponds to the bilinear form in Eq. (56) is given by:

$$(B_c)_{ji} = \int_{I_z}\int_{0}^{R}\int_{\theta_1}^{\omega} r^{(\alpha_i^{(R)}+\alpha_j^{(R)}-1)} \sum_{l,k=1}^{3} (\tilde{D}u)_k^j E_{kl} (\tilde{D}u)_l^i dr d\theta dz \tag{58}$$

$\alpha_i^{(R)}$ being the real part of the eigenpair, and $(Du)^j$ is a vector corresponding to the j-th eigenfunction and is given in Ref. [2].

The eigenstress tensor, having been derived from the eigenpairs, automatically satisfies the boundary conditions on all boundaries except Γ_R, so that the linear form in Eq. (57) degenerates into an integral over the cylindrical boundary Γ_R x I_z alone.

Replacing the vector u in Eq. (57) with the approximated finite element solution on Γ_3 x I_z, u_{FE}, the j-th term of the load vector corresponding to the linear form Eq. (57) becomes:

$$(F_c)_j = R\int_{I_z}\int_{\theta_1}^{\omega} \vec{u}^T [Q][E]\left(\vec{Du}^{(j)}\right)\Big|_{(r=R)} d\theta dz \tag{59}$$

where $[Q]$ is given in Eq. (49).

Solving Eq. (55), one obtains an approximation for the coefficients of the asymptotic expansion, the GSIFs. Numerical tests demonstrated that the rate of convergence of the GSIFs is as fast as the convergence of the strain energy, therefore the method is ''superconvergent". Analogous procedures will be needed for the computation of eigenpairs and stress intensity factors at vertex and vertex-edge singularities.

3.2.4 Thermal Loading: Computation of the TSIFs.

In [3] a mathematical analysis on the influence of the temperature field on the stress intensity factors is presented. The main results show that elastic bodies containing singular points subjected to steady-state heat distribution experience stress intensification determined by thermal stress intensity factors (TSIFs). These TSIFs are the first two coefficients of the asymptotic expansion in Eq. (1). The principle of complementary energy, together with the modified Steklov method and the p-version of the finite element method can be utilized, as shown in Section 2.3, for obtaining the TSIFs in a limit process as the integration radius around the singular point approaches zero. Although very good results can be obtained, it is necessary to refine the finite element mesh in the vicinity of the singular point. This is because the present method relies on the displacement field close to it. Importantly, the proposed method is applicable not only to singularities associated with crack tips, but also to multi-material interfaces and non-homogeneous materials. It has been shown also that for weak stress singularities the method has to be modified to include terms associated with the displacement field due to the singular temperature field around the singular point.

Once these terms are included, the integration radius can be enlarged to obtain good approximation for the TSIFs without the need for mesh refinement. The implications of the analysis on the computation of the TSIFs are the following:

(a) The most singular term in the stress tensor in the neighborhood of a singular point is independent of the asymptotic expansion of temperature.

(b) The TSIFs are independent of the thermal field in the vicinity of the singular point. Nevertheless, these TSIFs depend on the far thermal loading, which is the solution of the linear stationary heat transfer problem affected by the singular point.

(c) The TSIFs may be extracted using the modified Steklov method and the complementary energy method in a limit process as the integration radius approaches zero, without addressing the thermal distribution in the neighborhood of the singular point.

3.3 Schedule

It is estimated that the activities leading to the completion of the three-dimensional implementation will take two years. A Phase II STTR proposal was submitted to the Air Force Office of Scientific Research on September 12, 1996 with a detailed performance schedule.

4 Summary

All of the objectives set for the Phase I project have been achieved. Capabilities for the evaluation of the mechanical strength of electronic components subjected to thermal and mechanical loading was developed for two-dimensional applications. The implementation, based on recent technological advances, makes it possible to determine the natural straining modes and their intensities at singular points associated with multi-material interfaces.

The computational techniques were implemented in a two-dimensional setting as a module within the existing software infrastructure of Stress Check, which was developed by the small business concern (ESRD) over the past six years. Stress Check is based on the p- and hp-versions of the finite element method and has several innovative capabilities not available in other finite element programs. The new capabilities are available for professional use through Stress Check. The user-information is available in Chapter 12 of the user's manual of Stress Check [17].

The Phase I project also investigated the feasibility of the implementation of the computation of the eigenpairs that characterize the temperature and displacement fields in the vicinity of singularities caused by multi-material interfaces in three-dimensions. Successful completion of the activities to extend the current implementation into three-dimensions, will lay the groundwork for quantitative evaluation of the conditions that cause mechanical failure in electronic devices and composites. This technological development is an essential prerequisite to proper interpretation of experimental data in much the same way as the ability to compute stress intensity factors in linear

elastic fracture mechanics is an essential prerequisite to proper interpretation of experimentally obtained crack propagation data. This analytical capability, coupled with reference data obtained from simple experiments, will make it possible to evaluate design alternatives in the fields of electronic component design and composite materials technology. The capability will be made available for professional use through the finite element analysis software Stress Check. The new capability is expected to be of substantial interest to manufacturers of electronic components, aerospace companies, and their suppliers.

The project addressed the thermo-mechanical aspects of failure initiation in electronic components under the assumption that the natural straining modes of the linear thermoelastic problem characterize failure. It is expected that for many materials in the normal operating temperature range it will be possible to verify this assumption experimentally.

5 References

[1] Yosibash, Z. and Szabo, B. A. Numerical Analysis of Singularities in two-dimensions. Part 1: Computation of Eigenpairs. *Int. Jour. Numer. Meth. Engrg.*, Vol. 38, pp. 2055-2082 (1995).

[2] Yosibash, Z. and Szabo, B. A. Numerical Analysis of Singularities in two-dimensions. Part 2: Computation of Generalized Flux/Stress Intensity Factors. *Int. Jour. Numer. Meth. Engrg.*, Vol. 39 (3), pp. 409-434 (1996).

[3] Yosibash, Z. Numerical Thermo-Elastic Analysis of Singularities in Two-Dimensions. *International Journal of Fracture*, Vol. 74, pp. 341-361 (1996).

[4] Babuska, I. and Miller, A. The Post-processing Approach in Finite Element Method - Part 2: The Calculation of Stress Intensity Factors. *Int Jour. Num. Meth. Engrg.,* Vol. 20, pp. 1111-1129, (1984).

[5] Oh, H. S. and Babuska, I. P-Version of the Finite Element Method for the Elliptic Boundary Value Problem with Interfaces. *Computer Meth. Appl. Mech. Engrg., Vol* 97 (2), pp. 211-231 (1992).

[6] Szabo, B. A. and Babuska, I. *Finite Element Analysis.* John Wiley and Sons, Inc., 1991.

[7] Suo, Z. *Mechanics of Interface Fracture.* PhD Thesis, Harvard University, Cambridge, Massachusetts, 1989.

[8] Chen, D. H. Analysis of Singular Stress Field Around the Inclusion Corner Tip. *Engineering Fracture Mechanics*, Vol. 49 (4), pp. 553-546 (1994).

[9] Yosibash, Z. *Numerical Analysis of Singularities and First Derivatives for Elliptic Boundary Value Problems in Two-Dimensions*. D. Sc. dissertation, Sever Institute of Technology, Washington University, St. Louis, Missouri, 1994.

[10] Lee, K. and Cho, Y. H. Boundary Element Analysis of Thermal Stress Intensity Factors for Cusp Cracks. *Engineering Fracture Mechanics,* Vol. 37 (4), pp. 787-798 (1990).

[11] Prased, N. N. V., Aliabadi, M. H., and Rooke, D. P. The Dual Boundary Element Method for Thermoelastic Crack Problems. *International Journal of Fracture, Vol.* 66, pp. 255-272 (1994).

[12] Sumi, N. and Katayama, T. Thermal Stress Singularities at tips of Griffith Crack in a Finite Rectangular Plate. *Nuclear Eng. Desgn.,* Vol. 60, pp. 389-394 (1980).

[13] Anderson, B., Falk, U., Babuska, I. and Von-Petersdorff, T. Reliable Stress and Fracture Mechanics Analysis of Complex Components Using a h-p Version of FEM. *Int. Jour. Numer. Meth. Engrg*., Vol. 38, pp. 2135-2163 (1995).

[14] Babuska, I., Von-Petersdorff, T. and Anderson, B. Numerical Treatment of Vertex Singularities and Intensity Factors for Mixed Boundary Value Problems for the Laplace Equation in R^3. *SIAM. Jour. Numer. Analysis*, Vol. 31(5), pp. 1265-1288 (1994).

[15] Dauge, M. *Elliptic Boundary Value Problems in Corner Domains - Smoothness and Asymptotics of Solutions.* Lecture Notes in Mathematics 1341, Springer-Verlag, Heidelberg, 1988.

[16] Guo, B.and Oh, H.S. The Method of Auxiliary Mapping for the Finite Element Solutions of Elliptic Partial Differential Equations on Nonsmooth Domains in R^3. Preprint submitted for publication to *Mathematics of Computations, 1996.*

[17] Stress Check User's Manual, Release 2.2, October 1996. Engineering Software Research and Development, St. Louis, Missouri.